nature plants

Article

https://doi.org/10.1038/s41477-025-02011-y

Leaf venation network evolution across clades and scales

Received: 18 September 2024

Accepted: 25 April 2025

Published online: 06 June 2025

Check for updates

Ilaine Silveira Matos[1,2] ✉, Bradley Vu[1], Joseph Mann[1], Emily Xie[1], Srinivasan Madhavan[1], Satvik Sharma[1], Izzi Niewiadomski[1], Andrea Echevarria[1], Connor Tomaka[1], Sonoma Carlos[1], Monica Antonio[1], Ashley Chu[1], Meg Scudder[1], Nicole Yokota[1], Hailey J. Park[1,3], Natalie Vuong[4], Mickey Boakye[1], Miguel A. Duarte[5], Caroline Pechuzal[1], Luiza Maria T. Aparecido[6], Mia B. Franco[1], Ryan Jen Wong[1], Jocelyn Liu[1], Emily Guevara Heredia[5,7], Brad Boyle[8], Martha Ryan[9], Rafael E. Cárdenas[7], Brian J. Enquist[8], Diane M. Erwin[10], Holly Forbes[11], Kyle Dexter[12,13,14], Mark Fricker[15] & Benjamin W. Blonder[1]

Leaf venation architecture varies greatly among living and fossil plants. However, we still have a limited understanding of when, why and in which clades new architectures arose and how they impacted leaf functioning. Using data from 1,000 extant and extinct (fossil) plants, we reconstructed approximately 400 million years of venation evolution across clades and vein sizes. Overall, venation networks evolved from having fewer veins and less smooth loops to having more veins and smoother loops, but these changes only occurred in small and medium vein sizes. The diversity of architectural designs increased biphasically, first peaking in the Paleozoic, then decreasing during the Cretaceous, then increasing again in the Cenozoic, when recent angiosperm lineages initiated a second and ongoing phase of diversification. Vein evolution was not associated with temperature and CO_2 fluctuations but was associated with insect diversification. Our results highlight the complexity of the evolutionary trajectory and potential drivers of venation network architecture.

The approximately 400 million years of evolutionary history in vascular plant leaves has resulted in a diversity of venation network architectures in extant and extinct plants[1,2] (Fig. 1). Despite the importance of those architectural features to multiple leaf functions[3,4], many aspects of their evolution remain unresolved. This limits our capacity to assess the evolution of ecophysiology[1], reconstruct paleoclimate[5] and interpret plant-climate feedback across deep time[6].

Previous studies have reconstructed the evolution of individual venation traits, particularly minor vein density (VD)[1,7,8]. They revealed that an eightfold increase in minor VD in late angiosperm lineages led to a surge in photosynthetic capacity, with implications for terrestrial biogeochemistry and biodiversity[7–11]. Minor VD, however, is just one among many traits describing network architecture (Fig. 2). Many unknowns remain about when and in which clades the evolution of novel trait combinations originated[9,10] and whether the diversity of network architectures increased (by divergence) or decreased (by convergence or extinction) over time.

Venation traits vary systematically across vein sizes[3,4] and may also show different evolutionary lability, with traits in smaller veins thought to be more labile[3,11]. These differences suggest that venation traits could have followed distinct evolutionary trajectories across vein sizes[4], for example, smaller veins (for example, minor veins) evolving traits to optimize flow efficiency and larger veins (for example, major veins) developing features for mechanical strength[12]. Alternatively, complex architectures sometimes consist of highly integrated traits[13], such that a coordinated evolutionary response could exist across vein

A full list of affiliations appears at the end of the paper. ✉e-mail: ilaine.matos@gmail.com

https://doi.org/10.1038/s41477-025-02011-y

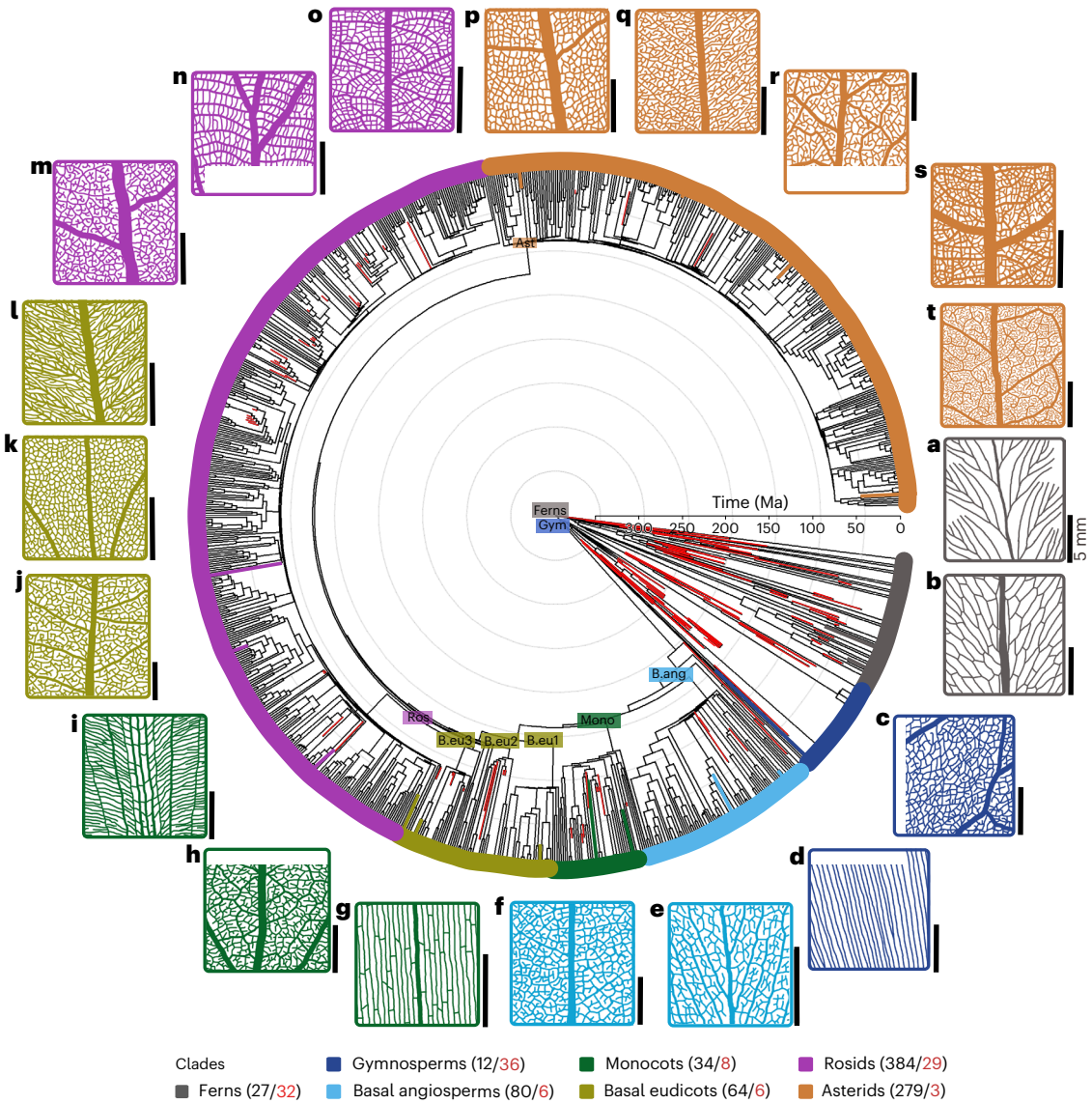

Fig. 1 | Time-calibrated phylogeny of 1,000 vascular plant taxa. Red branches indicate fossil taxa ($N = 120$), and black branches indicate extant taxa ($N = 880$). The other coloured branches indicate the taxa depicted in the outer images. Parenthetical numbers indicate the number of extant (black) and fossil (red) taxa sampled in each clade. Internal nodes for each clade are indicated by the labelled, coloured rectangles. The colours of the outer circles represent the clades depicted in the caption. The outer images are representative of taxa with distinct leaf venation network architectures. **a**, *Microlepia platyphylla* (Dennstaedtiaceae). **b**, *Onoclea sensibilis* (Onocleaceae). **c**, *Gnetum nodiflorum* (Gnetaceae). **d**, *Agathis lanceolata* (Araucariaceae). **e**, *Tasmannia lanceolata* (Winteraceae). **f**, *Umbellularia californica* (Lauraceae). **g**, *Barbacenia purpurea* (Velloziaceae). **h**, *Smilax hispida* (Smilacaceae). **i**, *Pollia crispata* (Commelinaceae). **j**, *Parvatia brunoniana* (Lardizabalaceae). **k**, *Synaphea dilatata* (Proteaceae). **l**, *Buxus harlandii* (Buxaceae). **m**, *Ungnadia speciosa* (Sapindaceae). **n**, *Luehea tessmannii* (Malvaceae). **o**, *Hua gabonii* (Huaceae). **p**, *Aextoxicon punctatum* (Aextoxicaceae). **q**, *Grenacheria beccariana* (Primulaceae). **r**, *Cavendishia guatemalensis* (Ericaceae). **s**, *Guettarda scabra* (Rubiaceae). **t**, *Phelline brachyphylla* (Phellinaceae). Note that in our analyses basal eudicots comprise three monophyletic groups (b.eu1–b.eu3). Scale bars, 5 mm. Supplementary Fig. 1 shows this tree with visible taxon names and node labels. Ast, asterids; Gym, gymnosperms; Ros, rosids; B.eu, basal eudicots; Mono, monocots; B.ang, basal angiosperms.

sizes (small, medium, large), vein orders (minor × major) and/or traits. Such hypotheses about independent versus coordinated venation evolution still remain largely untested, as previous studies have focused on a few venation traits, typically on subregions of leaves, and have included fossil taxa with limited temporal coverage[1,7,8].

The biotic and abiotic drivers of venation trait evolution are also uncertain. A decline in atmospheric carbon dioxide (CO_2) concentration during the Cretaceous is oftentimes linked to the evolution of networks with high minor VD[6,10]. Much less is known about which environmental conditions caused changes in other venation features, for example, in the density of larger veins or the degree of looping in the network architecture. Simulations suggest that, in response to frequent damage[14], networks develop loops to bypass damaged areas. Therefore, the evolution of looping networks or of non-minor veins architectural features could be linked to increased damage pressure from herbivore evolution[15] or to fluctuations in climate, but these hypotheses have not yet been formally tested.

Here we assembled venation networks for 1,000 extant ($N = 880$) and extinct ($N = 120$) plant taxa (Fig. 1 and Supplementary Fig. 1). Cleared leaf images or compression fossils representing whole (extant) or partial (extinct) leaves were traced and segmented, enabling extraction of multiple venation traits[3] (Fig. 2). By applying novel phylogenetic comparative methods[16], we were able to answer the following questions: (1) How did venation traits evolve across vein sizes (that is, small,

https://doi.org/10.1038/s41477-025-02011-y

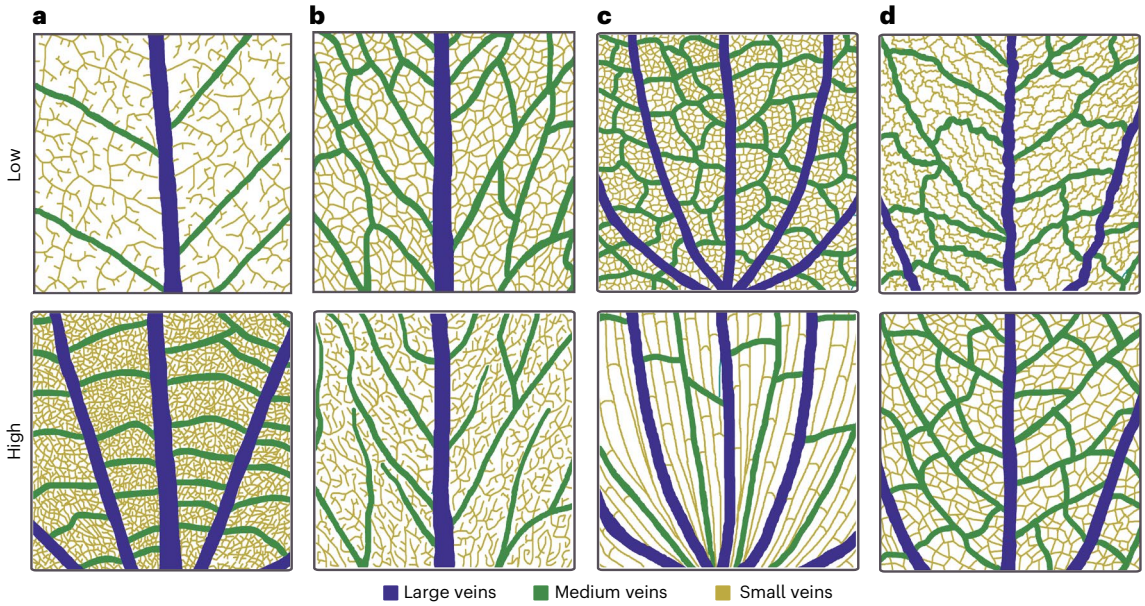

Fig. 2 | Examples of leaf networks with low and high values for four architecture traits. a, VD (mm mm^{-2}) quantifies the length of total vein segments per unit of leaf area, that is, if leaf networks have fewer (low VD) or more (high VD) veins per area. **b**, MST (dimensionless) describes the degree of reticulation or branching, that is, whether leaf networks have more loops (low MST) or fewer loops (high MST). **c**, Loop elongation ratio (ER) (dimensionless) describes the shape of the loops, that is, if loops are more circular (low ER) or more elongated (high ER). **d**, Loop CR (dimensionless) describes the degree of loop smoothness, that is, if loops are more (low CR) or less (high CR) smooth. All illustrations show networks with high or low values of each venation architecture trait across three vein size scales (large, medium and small vein sizes). However, architecture traits can also vary independently across scales; for example, a network can have branching large veins with low density but looping small veins with high density. This size classification into small, medium and large veins does not necessarily coincide with vein orders (for example, primary, secondary, tertiary).

medium, large veins) and major clades? (2) How did the occupancy of morphospace change over time? (3) How are each of climate and herbivory proxies correlated to leaf venation traits over time?

Results

Evolution of venation traits across clades and vein sizes

Using phylogenetic ridge regressions incorporating internal node constraints derived from fossils[14], we inferred the evolutionary trajectories of venation networks across major plant clades and vein sizes (Figs. 3 and 4 and Supplementary Data 1). Considering all vascular plants, leaf venation networks evolved from initially having fewer veins and less smooth loops (lower VD and circularity ratio (CR) at small and medium veins) to more complex networks with more veins (higher VD_{small} and VD_{medium}), smoother loops (higher CR_{small} and CR_{medium}) and fewer loops (higher minimum spanning tree ratio $(MST)_{small}$ and MST_{medium}; Fig. 3). Note that the decrease in MST_{small} over time does not suggest that leaves evolved towards completely non-reticulate networks (as MST_{small} did not evolve to 1, which would indicate fully branched networks). Instead, the trend in MST_{small} suggests the evolution of networks that still have loops but might also have a larger proportion of internal free-ending veins (FEVs). Supporting this idea, we further calculated the density of FEVs for our investigated species (Supplementary Note 1) and found a significant temporal trend of increased FEV density over time for all vascular plants pooled together.

Significant evolutionary trends were only observed at small and medium vein sizes, while the architecture of larger veins has not shifted directionally over the approximately 400 million years of vascular plant evolution. Even though we found small and significant differences in evolutionary rates of venation traits across vein sizes (Extended Data Fig. 1), there was no evidence of slower trait evolution in larger veins for any of the traits evaluated. That is, evolutionary rates of venation traits in larger veins either did not differ or were actually higher (not lower) when compared with small/medium veins. Overall, our sensitivity analysis (Supplementary Data 2) indicated that these observed patterns were robust to subsampling and uncertainties associated with phylogenetic placement and age of fossils.

Importantly, in some samples, we were unable to segment very small veins (veins with width <10 µm). Therefore, FEV density calculated here might not have captured all free ending veinlets in all species, nor were the FEVs in this study defined based on terms of their developmental features. Arguably, even if minor veins are missing in some samples, our estimates of vein traits for larger vein scales are still relevant—particularly because their evolution has been largely unexplored in previous studies. In addition, our vein size classification into small, medium and large veins (see Methods for more details) does not necessarily coincide with the traditional classification of primary (major), secondary and tertiary (minor) veins nor considers vein tapering (Extended Data Fig. 2).

Despite those general patterns, when we looked at the evolutionary trends within each major plant clade, we found that clades sometimes followed distinct trajectories in terms of both magnitude and direction of trait change over time (Fig. 4 and Extended Data Fig. 2). For example, while gymnosperms, monocots and rosids showed a clear temporal increase in VD (Extended Data Fig. 3a,b), no significant trend in VD was observed in other plant clades (Supplementary Data 3). Similarly, networks evolved fewer loops at small and/or medium veins in most clades, except in monocots and rosids which showed the opposite pattern of evolution (Extended Data Fig. 3d,e). Together, these results show that directional evolution of venation traits occurred for some but not all components of network architecture and only for certain clades and vein sizes.

Changes in morphospace occupancy over time

Using a principal component analysis (PCA) with the reconstructed venation trait values (Fig. 5a), we calculated two complementary metrics of morphospace disparity that described the position (median centroids) and the extent (sum variances) of space occupied by each clade. We then found that ferns, gymnosperms and monocots explored a higher diversity of architectures than any eudicot clade (Fig. 5b,c).

https://doi.org/10.1038/s41477-025-02011-y

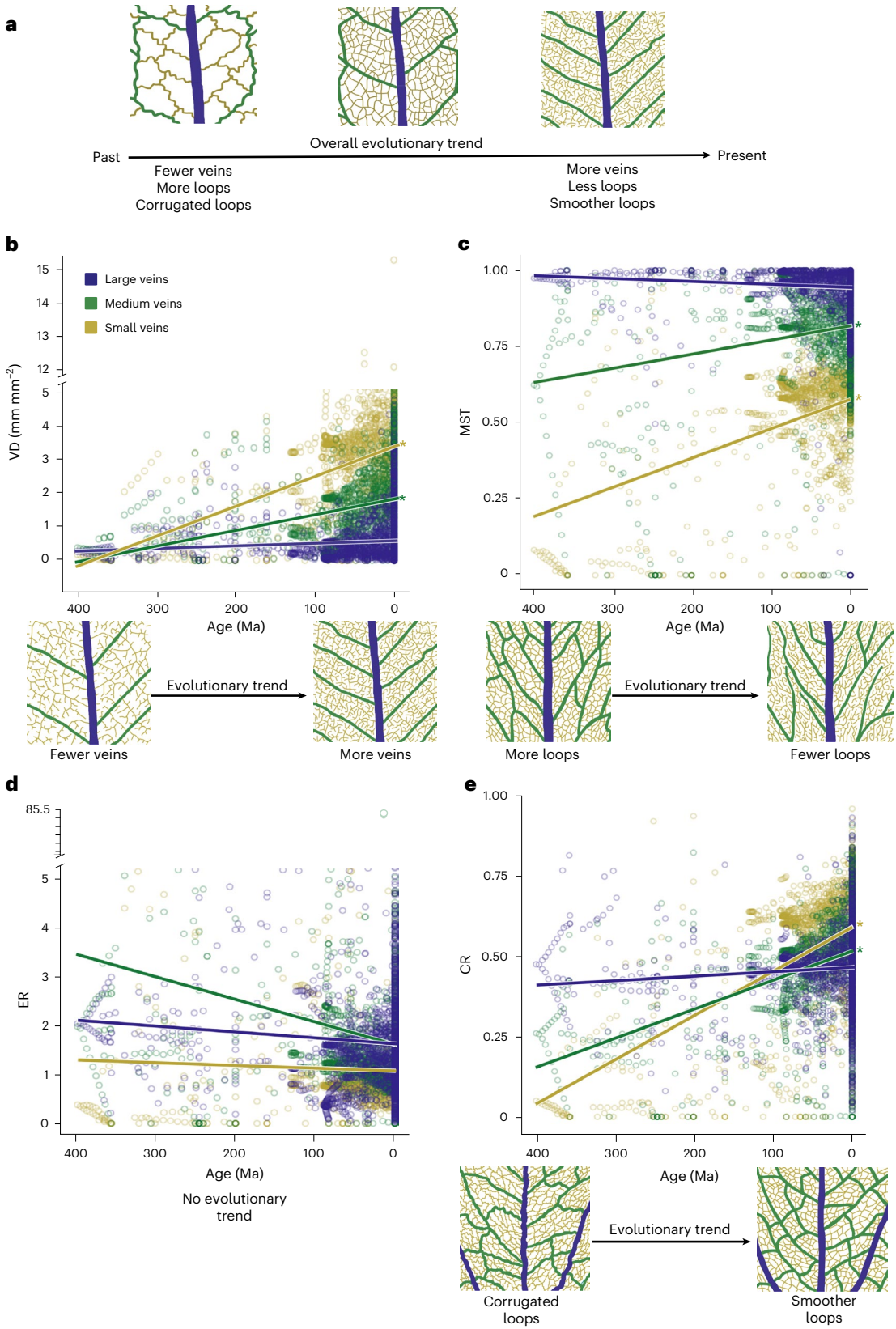

Fig. 3 | Evolutionary trends in four leaf venation architecture traits across vein sizes (small, medium, large) for the entire phylogeny of vascular plants. **a**, Summary of the overall evolutionary trends of venation architectural traits. **b**, VD (mm mm^{-2}). **c**, MST (dimensionless). **d**, Loop ER (dimensionless). **e**, Loop CR (dimensionless). Points represent measured trait values at phylogenetic tree tips and maximum likelihood ancestral state estimates of internal nodes. Lines show phylogenetic ridge regression estimates of linear trends in mean trait values over time. A single asterisk ('*') on the right side indicates a significant trend ($\alpha = 0.05$). Insets: the significant trends. Insets were not included for ER, as no significant directional trend was detected for this trait.

https://doi.org/10.1038/s41477-025-02011-y

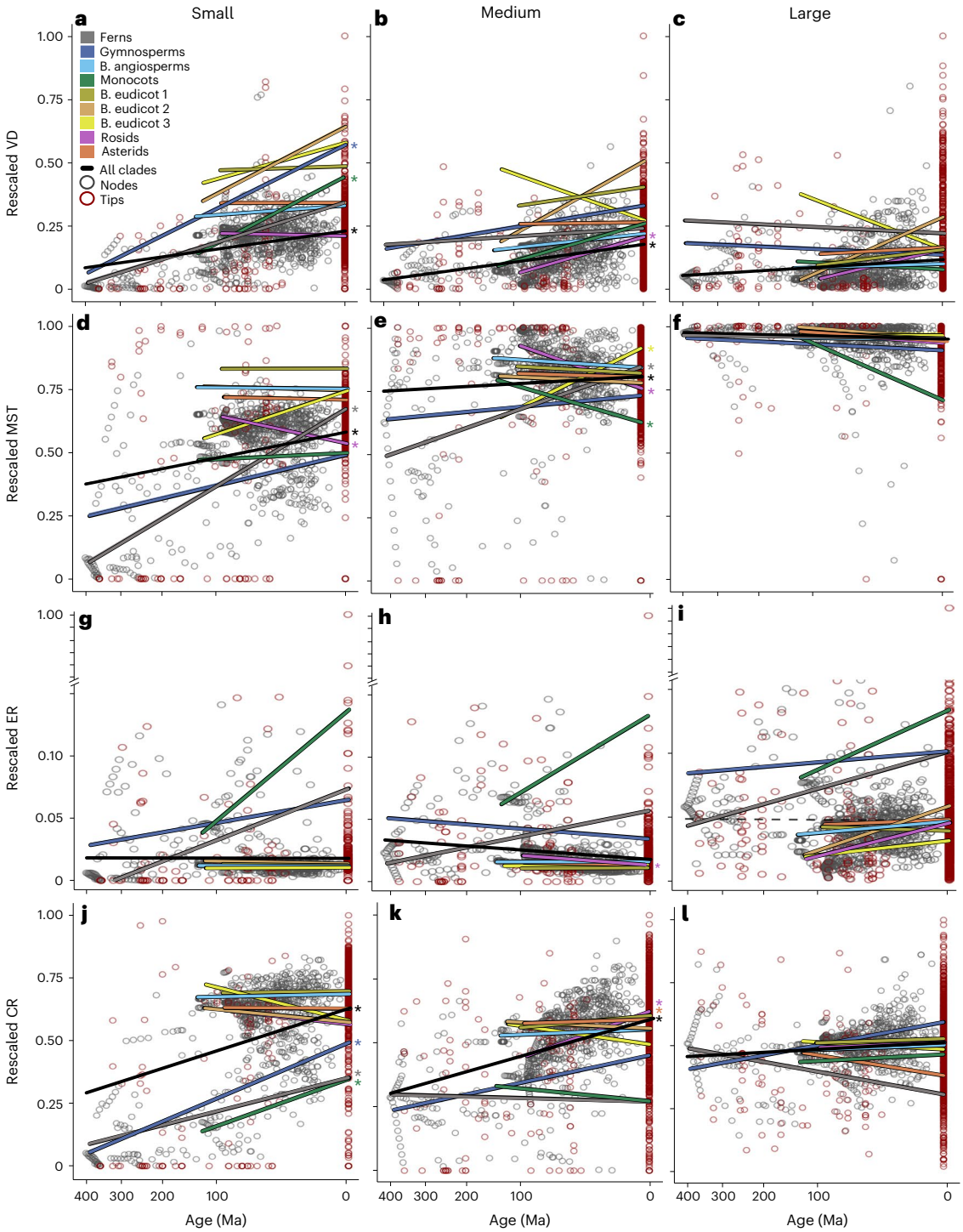

Fig. 4 | Evolutionary trends in individual leaf venation architecture traits across vein sizes and plant clades. a–**c**, VD at small (**a**), medium (**b**) and large (**c**) veins. **d**–**f**, MST at small (**d**), medium (**e**) and large (**f**) veins. **g**–**i**, Loop ER at small (**g**), medium (**h**) and large (**i**) veins. **j**–**l**, Loop CR at small (**j**), medium (**k**) and large (**l**) veins. Red circles represent actual trait values, and grey circles represent ancestral state estimates of internal nodes. The regression of mean trait values through time for all clades together is indicated by a black solid line. A single asterisk ('*') indicates significant evolutionary trends for the clade of that colour. All venation architecture traits were rescaled to vary between 0 and 1 for ease of comparison.

When we conducted a disparity-through-time (DTT) analysis at ~10 million year time slices (Supplementary Data 4), we found that the disparity in architectures showed a biphasic increase (Fig. 5d) and followed a model of evolution constrained towards an optimum (that is, Ornstein–Uhlenbeck model; Supplementary Data 5). That is, vascular plants explored a greater diversity of architectures midway through their evolutionary history, with a peak in disparity in the Mesozoic period (~200–150 million years ago (Ma)), when ferns and gymnosperms dominated the terrestrial flora. Then, with the advent of angiosperms during the Cretaceous (~125–80 Ma), the disparity narrowed down to a more limited variety of venation trait combinations. It was only after the Cretaceous–Paleogene mass extinction (~66 Ma) that the disparity started to increase a second time—following the diversification of extant angiosperm lineages. A subsequent analysis of

https://doi.org/10.1038/s41477-025-02011-y

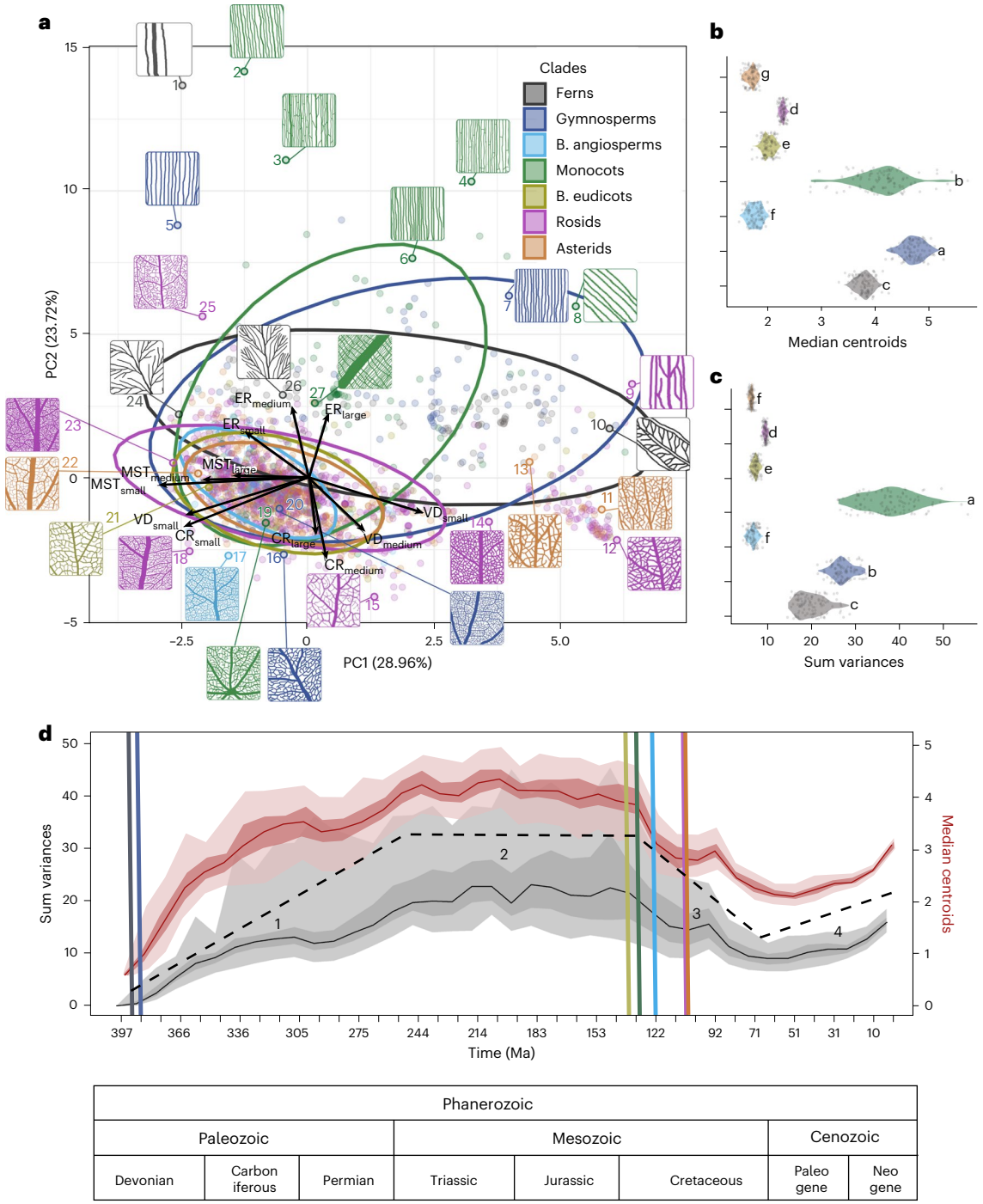

Fig. 5 | The venation architectural space of vascular plants and its variation over time. a, First (PC1) and second (PC2) principal components of leaf venation architecture traits (VD, MST, ER, CR) at three vein sizes (small, medium, large) across plant clades. **b**,**c**, Differences across plant clades in two metrics of disparity describing the position occupied (**b**) (that is, median centroids) and the extent of space occupied (**c**) (that is, sum variances). **d**, Temporal changes in the venation architectural space occupation under a gradual model of evolution. In **a**, venation trait values were obtained by collating ancestral state estimates to measured trait values at the tree tips; 95% confidence ellipses enclose the data at each clade. In **b** and **c**, letters indicate significant difference ($\alpha = 0.05$) between clades according to nonparametric multivariate analysis of variance tests. In **d**, black and red lines indicate the median disparity metric value for each approximately 10 million year time slices and the corresponding 50% and 95% confidence intervals. The coloured vertical lines indicate the approximate age of origin of each vascular plant clade. The dashed black line indicates the different phases (phases 1–4) of disparity variation over time. Note that **a** only depicts a 2-dimensional architectural space, while the 2 disparity metrics (in **b**–**d**) actually were calculated using the 12-dimensional space. Species depicted in **a**: 1, *Equisetum telmateia* (Equisetaceae); 2, *Puya alpestris* (Bromeliaceae); 3, *Astelia banksii* (Asteliaceae); 4, *Luzula nivea* (Juncaceae); 5, *Ginkgoites* sp. (Ginkgoaceae); 6, *Typha latissima* (Typhaceae); 7, *Nilssonia* sp. (Nilssoniaceae); 8, *Triantha glutinosa* (Tofieldiaceae); 9, *Floerkea prosperpinacoides* (Limnanthaceae); 10, *Pteridium esculetum* (Dennstaedtiaceae); 11, *Baccharis sergilioides* (Asteraceae); 12, *Sagenopteris philippsii* (Caytoniaceae); 13, *Fouquieria splendens* (Fouquieriaceae); 14, *Castanopsis chrysophylla* (Fagaceae); 15, *Colubrina glabra* (Crossosomataceae); 16, *Gnetum gnemonoides* (Gnetaceae); 17, *Beilschmiedia erythrophloea* (Lauraceae); 18, *Khaya grandifoliola* (Meliaceae); 19, *Dioscorea polystachya* (Dioscoreaceae); 20, *Cylista preussii* (Fabaceae); 21, *Hamamelis virginiana* (Hamamelidaceae); 22, *Scrophularia nodosa* (Scrophulariaceae); 23, *Fagus longifolia* (Fagaceae); 24, *Dryopteris remota* (Dryopteridaceae); 25, *Helwingia chinensis* (Aquifoliaceae); 26, *Microlepia platypoda* (Dennstaedtiaceae); 27, *Attalea rostrata* (Arecaceae).

https://doi.org/10.1038/s41477-025-02011-y

the temporal dynamics in disparity for each separate clade (Extended Data Fig. 4) showed that (1) in eudicot clades, especially monocots, disparity consistently increased over time, and (2) in ferns, disparity plateaued approximately 200 Ma (Extended Data Fig. 4). Those trends were similar in both gradual (Extended Data Fig. 4) and punctuated (Supplementary Fig. 2) models of evolution.

Overall, our findings not only highlight the higher diversity of venation architectures explored by early-diverging and now-extinct fern and gymnosperm species (Extended Data Fig. 5) but also suggest that present-day lineages of angiosperms are still undergoing a second wave of diversification in venation architecture (that is, no saturation of morphospace).

Correlations between climate, herbivory and venation evolution

We compared the reconstructed temporal trajectories in venation traits and disparity metrics, with published time series of paleoclimate (that is, temperature[17] and atmospheric CO_2 (ref. 18)) and herbivory proxy variables (that is, global insect diversification rates)[19] (Fig. 6). Although it is true that most insects are not phytophagous (~25–35% of insect species are herbivores), previous studies have indicated herbivory as a major driver of insect diversification in many major insect orders[19], so in the absence of data on diversification rates solely for phytophagous insects, we used global rates of diversification for all major insect groups as a proxy for insect herbivory pressure. Using generalized least squares (GLS) regression, a positive relationship was observed between morphospace disparity (median of centroids) and certain venation traits (VD, CR, MST) in small and medium vein sizes with global insect diversification rates (Extended Data Fig. 6). Additional regression analysis showed no evidence that the presence of leaf exudates (that is, resins and latex) influence these correlations (Supplementary Note 2). However, we found no significant correlation between venation traits and the climatic proxies investigated (Supplementary Data 6), except for a weak relationship between CO_2 concentrations and CR in gymnosperms (Supplementary Fig. 3). Our regression results also showed no evidence of a significant interaction between CO_2 and temperature in influencing venation traits over time, except for MST (Supplementary Data 6). Interestingly, our temporal analysis also showed that the Late Devonian and the Triassic–Jurassic mass extinctions were not associated with major impacts on venation evolution, whereas the Permian–Triassic event was associated with a decline in venation trait values, particularly at small vein sizes (Fig. 6a–c).

These results underscore the complex multidimensional drivers of venation architecture evolution and highlight a potential role of insect herbivory pressure on the evolution of different architecture designs. These results also show that over larger temporal or phylogenetic scales, previously reported single-variable trait–climate relationships become weak (for example, VD and temperature).

Discussion

Using a dataset of 1,000 (extant and extinct) species' venation networks and recently developed methods for extracting multiscale venation traits[3,19] and performing ancestral state reconstructions[16], we reconstructed the approximately 400 million year history of leaf venation architecture evolution. Our major findings were (1) venation networks evolved from initially having fewer veins with corrugated loops to having more veins, smoother loops (Fig. 3a)

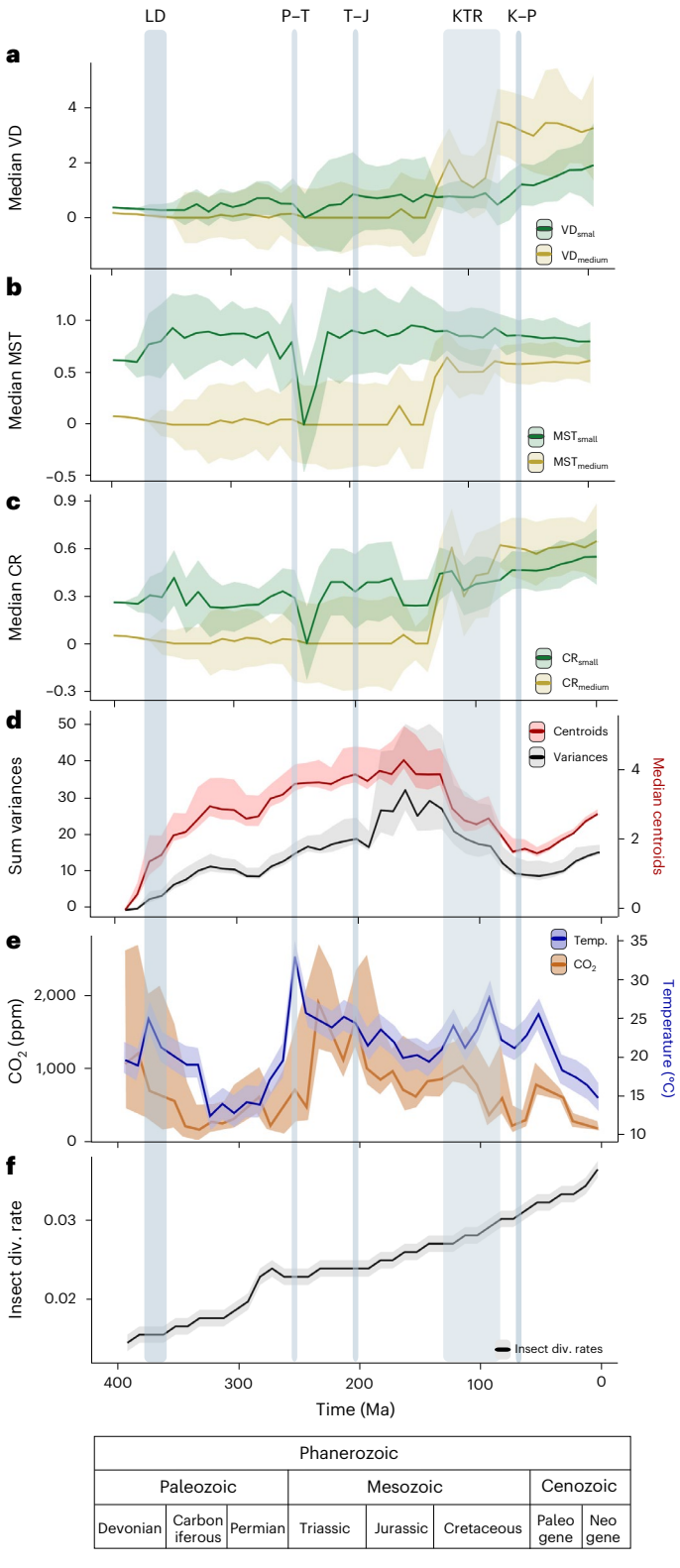

Fig. 6 | Variation in leaf venation architecture compared to abiotic and biotic proxies across the Phanerozoic eon. a–c, Ancestral state reconstructions of VD (**a**), MST (**b**) and loop CR (**c**) at two scaled vein sizes (small and medium). **d**, Two metrics of venation architecture disparity, sum variances and median centroids. **e**, Abiotic proxies: global reconstruction of atmospheric average temperature (Temp.)[17] and atmospheric CO_2 concentration[18]. **f**, Biotic proxies: global insect diversification rates (Insect div. rates)[19]. Temporal trajectories for loop ER and for large veins are not shown because they did not show significant evolutionary trends. In all panels, lines represent the median values averaged over approximately 10 million year time bins with standard deviation (in **a**–**c** and **f**) or 95% confidence interval (in **d** and **e**). Shaded vertical bars indicate the time of important geological events: LD, Late Devonian mass extinction; P–T, Permian–Triassic mass extinction; T–J, Triassic–Jurassic mass extinction; KTR, Cretaceous Terrestrial Revolution; K–P, Cretaceous–Paleogene mass extinction.

and more internal FEVs (Supplementary Note 1); (2) the evolution of venation architectural designs followed a biphasic trajectory, with ferns and early-diverging seed plants first filling the boundaries of viable trait combinations and then with angiosperm lineages bringing architectural innovations that initiated a second and ongoing phase of interior morphospace exploration (Fig. 5d); and (3) insect diversification rate was correlated with venation traits over time, suggesting that biotic interactions could have been an important factor influencing venation architecture diversification over time (Fig. 6). These results provide a clearer understanding of leaf evolution in several areas that we explore further below.

Evolution of venation networks beyond minor VD

Independent evolution of highly dense vein networks (in magnoliids, monocots and eudicots) has been documented before in studies using smaller datasets (N = 307–504), consisting mostly of angiosperm species[1,7,8]. Likewise, previous studies using stratigraphic distributions and qualitative venation characteristics have proposed a repeated differentiation from single-veined networks to dichotomously branching to looping networks with FEVs, in both ferns and seed plant lineages, via convergent evolution[9]. Here we re-evaluated those results using quantitative multiscale venation traits combined with modern phylogenetic comparative methods[16,20] applied to a wider phylogenetic tree (N = 1,000 taxa). We not only confirmed the existence of directional trends in VD and other important traits but also, for the first time, showed that temporal changes in small and medium veins—but not in larger veins—were responsible for those evolutionary trends (Fig. 3). At least for the four venation traits evaluated here, we found no evidence of slower evolution in larger veins (Extended Data Fig. 1). In fact, for some traits (that is, ER and CR) evolutionary rates were even higher (not lower) in larger veins. Therefore, the absence of directional changes in larger veins might not be linked to a lower evolutionary lability; rather it may stem from developmental or biophysical constraints. Unlike the minor veins, which are formed throughout the rapid leaf expansion phase and can develop into a wide range of final VDs and architectures, the major veins are formed earlier during leaf development and are constrained to a narrower variety of forms, which are more strictly dependent on the total leaf area[2,21].

Multiple possible selective forces for venation evolution

These findings for directional temporal trends open questions about the underlying selective forces for leaf veins evolution. One possibility is that leaf networks evolved towards architectural traits linked to higher flow efficiency, at least in angiosperm lineages, as previously proposed[1,7,22]. In modern plants, these traits are key determinants of leaf hydraulic capacity. They influence plant transpiration and photosynthetic rates[2] because a larger density of smaller veins, including FEVs, decreases the distance of transport through the mesophyll and thereby decreases the overall hydraulic resistance of the leaf[23]. In addition, network traits might have evolved to support other critical leaf functions, including mechanical support, resistance and resilience to damage[3,4,24,25]. For example, a higher density of small veins may provide an advantage against herbivory, forcing insects to expend more energy to cut through more veins, and may also provide redundant pathways to bypass damaged areas[26]. This idea is corroborated by our finding of a consistent relationship between insect diversification rates and venation traits over time, suggesting that herbivory pressure could have been a potential driver of venation architecture diversification (see below)—although further studies are needed to test this hypothesis. Although the functional significance of loop CR is yet to be determined[3,24], the network evolution towards smoother loops in small and medium vein sizes reflect a decrease in the relative allocation of vein perimeter relative to loop area over time[24]. This trend in CR_{small} and CR_{medium} could have led to a reduction in the surface area for water exchange between minor veins and the mesophyll but was likely compensated by the simultaneous increase in the proportion of FEVs. This may suggest that FEVs, rather than more corrugated loops, provide a more efficient connection for water flow from the terminal xylem to the mesophyll[27].

Expansions and contractions in the venation morphospace

The first 200 million years of venation evolution was characterized by a gradual expansion of the morphospace, with ferns and gymnosperms slowly exploring new architectures (Fig. 5d), for example, ranging from dichotomizing to looping networks and from single-vein order to hierarchical networks (with two or more distinct vein sizes or orders; see examples in Extended Data Fig. 5). By the Triassic–Jurassic boundary, disparity reached its maximum value and then stabilized, likely because these non-flowering plants reached the limits of morphological and developmental variation for leaf venation under marginal leaf growth (that is, where cell divisions are restricted to the leaf margins)[9]. During the Cretaceous, amid the Cretaceous Terrestrial Revolution when the Earth witnessed a rapid phylogenetic divergence of angiosperm families[15], disparity decreased rapidly. Two distinct processes could have been responsible for that decline in the diversity of venation architectures. First, a sudden increase in the extinction rates of ferns in the Late Cretaceous led to a collapse in fern diversity, resulting in a loss of architectural designs that were unique to this group[25]. Second, the rise of angiosperms catalysed a shift from plants with leaf-borne reproductive structures to plants where the reproductive and vegetative functions were segregated into separate structures, and a transition from marginal to diffuse leaf growth (that is, where cell divisions are dispersed throughout the leaf). Those functional and developmental changes may have led to a greater functional specialization and thereby a reduction in the diversity of venation patterns (that is, narrowing in the morphospace occupation) in seed plants[10,28,29]. That is, with the advent of angiosperms, network diversification occurred within a more limited range of the morphospace with a high-fitness trait combination. Simultaneously, some of the more extreme architectures (at the morphospace edges) of non-flowering plants may no longer have been competitive and eventually disappeared (for example, the extinct pteridosperms), even though other extreme architectures were retained until the present time (for example, *Ginkgo*).

It was only after the Cretaceous–Paleogene mass extinction that the disparity in venation architecture started increasing again in tandem with the radiation of extant angiosperms lineages[30,31]. Those new lineages developed the complex architectural designs dominant in the modern world, characterized by hierarchical orders of reticulate veins (that is, loops within loops) and dispersed, internal free-vein endings. Although similar architectural designs have evolved at least three times in non-angiosperm seed plants (for example, Gnetales and Gigantopterids) and at least ten times among extant ferns (for example, Dipterids and Polypods)[9], it was only in those later-diverging angiosperm lineages that hierarchical reticulate networks became common. This is likely because the late angiosperm transitions from tracheids to xylem vessels[7,32], and from scalariform to simple perforation plates[33], reduced the resistance to water flow inside the venation system, thus allowing the miniaturization of veins[7] and the development of more and more complex networks. It is worth noting that the development of the 'striate' parallel venation, typical of monocots, which is composed of several orders of longitudinal veins with small transverse veins connecting them[34], allowed eudicot plants to explore novel areas of morphospace, also largely contributing to the increase in disparity from the Cenozoic towards the present. An increase in disparity followed by a saturation of morphological potential is a common evolutionary pattern, observed both in plants and animals[35,36]. The fact that the second phase of increasing disparity in vascular plants has still not levelled off suggests that extant plant lineages have yet to explore new viable trait combinations.

Linkages between vein evolution, herbivory and climate

Despite the known mechanistic feedbacks between plants, CO_2 concentrations and temperature[37] mediated by VD and other venation traits[24], we found no evidence of a strong relationship between venation traits and those climatic factors over time, neither for vascular plants as a whole nor for each clade separately. For example, although global CO_2 concentrations and temperatures fluctuated widely during the first 250 million years of vascular plant evolution, VD and other venation traits remained relatively unchanged over this period. Because CO_2 and temperature fluctuations may interact with other important environmental factors (for example, precipitation amount and seasonality) not considered in this study, it may be hard to disentangle the individual effect of climatic factors on venation trait evolution.

Instead of being spurred by changes in climatic conditions, the evolutionary transformations observed in venation architecture could have been a response to altered herbivory pressure, as suggested by the association found in this study between different venation traits and global insect diversification rates. Insects and plants have been interacting since their origins, with those interactions driving the evolution of a notable taxonomic diversity in both groups[38]. Because 80% of herbivory damage in terms of leaf biomass is carried out by insects[39], an increase in the diversity and abundance of phytophagous insects could have imposed selection on leaves for higher resistance or resilience to damage. This could have been achieved, for example, by developing more veins (so insects would spend more energy cutting through veins[2]) and/or more loops (so water or latex could flow around damaged areas[14]). Here we were not able to differentiate the diversification rates of phytophagous versus non-phytophagous insects. We also did not consider evolutionary rates of other herbivores such as dinosaurs or mammals, but they might also be important for venation evolution.

Our broad-scale correlational study cannot conclusively support or reject any of these hypotheses but highlights the value of further investigating each. It is also possible that observed correlations between variables are caused by an unmeasured third variable. For example, minor VD increased with angiosperm diversification, and this could have been coupled with insect diversification via insect–plant pollination coevolution, rather than by insect herbivory (but see ref. 40). In addition, insect herbivory could have been an incidental influence on leaf venation evolution when compared to other factors driving venation evolution (for example, related to photosynthetic machinery, stomata), particularly because resistance or resilience to herbivory damage can be achieved by a range of adaptations, such as chemical defences (for example, secondary metabolites) and morphological barriers (for example, trichomes and spines) that are independent of venation traits[41]. Therefore, further studies examining how changes in venation traits are related to insect damage observed across the fossil leaf record[38] will be crucial to elucidate to what extent the correlations observed here reflect causal links between the diversification of insects and venation networks. Nevertheless, our dataset provides a first resource for future tests of biotic versus abiotic factors influencing network evolution.

Conclusions

This study provided an updated and data-rich perspective on leaf venation networks over 400 million years of time. It showed the contingency, complexity, scale dependence and nonlinearity of the evolutionary process, building a more detailed understanding of plant evolution relative to previous studies[1,8,23]. The hypotheses and correlations identified here, especially around herbivore evolution, will require further assessment but highlight the diversity of factors that may have shaped leaf evolution.

Methods

Obtaining images of leaf venation networks

We compiled 1,000 leaf images of extant (N = 880) and fossil (N = 120) species, distributed in 784 genera, 325 families and 90 orders (Supplementary Data 7). To create this unique dataset, we brought together samples from multiple collections.

Images of extant species were selected from the following: (1) Smithsonian National Cleared Leaf Collection, comprises 7,000 images available at https://collections.peabody.yale.edu/pb/nclc/; (2) University of California Museum of Paleontology (UCMP) Cleared Leaf Collection, comprises over 2,000 samples, including the Daniel I. Axelrod collection. Low-resolution images of some samples are available at https://ucmp.berkeley.edu/collections/paleobotany-collection/. Other samples were imaged at high resolution for this study; (3) Wilf collection[42], an open-access database of 26,176 leaf images; and (4) Macrosystem Ecology Laboratory at Berkeley collection, a database of 326 leaf images collected from Costa Rica, Ghana, Ecuador and the United States, including the University of California Botanical Garden (UCBG) at Berkeley. Our previous work[43,44] provides a full description of how Macrosystem Ecology Laboratory at Berkeley leaf samples were collected, cleared and imaged.

We evaluated all leaf images from these collections to determine which samples were suitable for our work. We selected only high-contrast and high-resolution images showing the whole leaf or with at least 75% of the leaf area present and with no major damage (for example, tears, holes, folds, bubbles, herbivory or material deterioration). For many monocot species, leaves were too long (>30 cm) to be wholly imaged, so a leaf segment representing approximately 20–50% of the total leaf area was analysed. Due to the variable resolution of the leaf images, our study was able to accurately resolve any vein with width ≥10 µm but occasionally missed small veins.

Images of extinct species were compiled from compression leaf fossil images from the following: (1) Yale Peabody Museum (https://peabody.yale.edu/), 4,300 imaged specimens, including Triassic and late Cretaceous floras from Arizona, New York, New Jersey and southern New England, available at the Global Biodiversity Information Facility (www.gbif.org); (2) Natural History Museum of Berlin (https://www.museumfuernaturkunde.berlin/), 29,826 fossil records from the Paleozoic to Cenozoic eras, also available at the Global Biodiversity Information Facility; (3) UCMP, approximately 12,000 fossil specimens available at https://ucmpdb.berkeley.edu/; (4) Illinois State Museum (https://www.illinoisstatemuseum.org/), 600 samples, including many Carboniferous fossils from the Mazon Creek formation; (5) Florida Museum (https://www.floridamuseum.ufl.edu/), approximately 250,000 specimens, ranging from the Proterozoic to the Pleistocene; and (6) University of Alberta Paleobotanical Collection, approximately 127,000 fossil specimens, available at https://search.museums.ualberta.ca/. In addition to those museum collections, we also sampled images of fossil leaves from the Wilf collection[42], which compiled 4,076 samples dated from Late Cretaceous to Eocene, including specimens from the Florissant Fossil Beds National Monument (late Eocene, Colorado, USA). Although leaf fossils are abundant in many depositional settings, the preservation of whole-leaf venation networks in fossils is rare. Thus, instead of whole leaves, we sampled leaf sections (ranging from 19 to 32,000 mm^2) from any leaf fossil image where tertiary or smaller veins were distinguishable. We also only retained fossil samples whose taxonomic identity and age could be retrieved, as this information was required for grafting fossil taxa to the phylogenetic tree ('Obtaining the phylogenetic tree of extant and fossil taxa' section). After inspecting all fossil images from these databases, we noticed an absence of samples from the Jurassic period. To fill this gap, we conducted a targeted literature search on the 'Google Scholar' database using the keywords 'Jurassic leaf fossil*', and found 7 peer-reviewed papers[45–51] from which we extracted 20 traceable leaf fossil images. We recognize that our survey of fossils is not exhaustive, and it is potentially biased towards taxa more likely to fossilize well. For example, the fossil record is biased against the preservation of taxa with low leaf mass per area, as these leaves tend to be mechanically damaged before fossilization[52]. Because low leaf mass per area can be linked to lower VD, particularly of larger

veins[3], VD_{large} could be underrepresented in our fossil dataset. Despite those limitations, our fossil dataset yielded key coverage of important internal nodes, ranging in age from 11.6 to 358.9 Ma, the time period of vascular land plant evolution.

When compiling leaf images, we aimed to maximize phylogenetic coverage by sampling species from all major vascular plant clades, including the following: (1) ferns, (2) gymnosperms (including Bennettitales, Caytoniales, Cordaitanthales, Medullosales), (3) basal angiosperms (including Amborellales, Nymphaeales, Austrobaileyales, Chloranthales, Magnoliids), (4) monocots (including Commelinids), (5) basal eudicots (including Ranunculales, Proteales, Trochodendrales, Buxales, Gunnerales, Dilleniales, Saxifragales), (6) rosids and (7) asterids. We limited our analysis to one leaf per species, so our study does not address trait intraspecific variation. This approach is justified as our study focuses on interspecific trait variation across the plant phylogeny.

Obtaining the phylogenetic tree of extant and fossil taxa

We assembled a time-calibrated phylogenetic supertree for all 1,000 vascular plant species evaluated in this study (Fig. 1 and Supplementary Fig. 1). First, we used the R package 'U.Taxostand' version 1.0[53] to standardize spellings and nomenclature for all extant species names, following the World Plants (worldplants.de) database and the Angiosperm Phylogeny Group IV classification[54]. Similarly, fossil names were standardized following the Paleobiology (paleobiodb.org) and Fossilworks (fossilworks.org) databases. After nomenclature standardization, we built a phylogenetic tree for all extant species using the 'V.PhyloMaker2' R package version 2.0[55] and the 'GBOTB.extended.WP.tre' mega-tree.

Next, to graft our fossil species to the tree, we used the function 'tree.merger' from the 'RRphylo' R package[20]. This function allows adding individual species (that is, our fossil species) to a backbone phylogeny (that is, our phylogenetic tree of extant species), while also automatically recalibrating the tree based on age values provided for specific nodes and/or tips (that is, fossil species last appearance age). To properly attach the fossil species, the tree.merger function requires the following: (1) name of the fossil species; (2) fossil's sister taxon(a) (that is, the fossil closest relative(s) present in the pre-existing tree); (3) fossil estimated last appearance age; and, optionally, (4) the estimated age of the parent node (that is, age of the node the fossil species descend from). For example, the backbone tree included the extant species *Betula occidentalis*, so the fossil species *Betula leopoldae* was grafted in this same genus, and all its parent nodes were recalibrated to consider the fossil species last appearance age at 38 Ma (Supplementary Data 8).

The information necessary for fossil grafting was obtained from the Paleobiology and Fossilworks databases, and the tree root age was placed in the Devonian, at 400.78 Ma. The ages of the internal nodes encompassing each of our seven major plant clades were also recalibrated using median estimated ages extracted from 'TimeTree' database[56]. In a few cases, information in those databases were outdated and replaced with split age estimates reported in more recent sources[57]. All information used for fossil grafting and tree calibration are available in Supplementary Data 8. Uncertainty in tips and node ages were later accounted for in our analysis ('Identifying evolutionary trends in venation traits' section) via bootstrapping methods using the 'overfitRR' function[58] from the RRphylo R package version 3.0.

Extracting venation architectural traits

We used GIMP version 2.10.32 (https://www.gimp.org/downloads/) and ImageJ version 1.53t (https://imagej.nih.gov/) to pre-process all leaf images. Image pre-processing involved cropping the leaf image, preparing masks to delineate leaf boundaries and determining image resolution, which ranged from 17 to 243 pixels mm^{-1} in extant species and from 14.4 to 175 pixels mm^{-1} in fossil species (Supplementary Data 7). For some species with a large midrib (that is, midvein), a mask of the midrib was also prepared to prevent it from splitting into multiple segments during the network extraction. After pre-processing, leaf image segmentation (that is, conversion of a coloured leaf cleared image into a binary image where veins pixels are shown in white and non-veins pixels are shown in black) was done automatically using LeafVeinCNN program versions 1.0.7 (ref. 59) and 2.12 (ref. 43). We configured LeafVeinCNN to use an ensemble average of three convolutional neural network predictions (CNNs) to segment veins. For leaf images that did not have a good colour contrast or had parallel venation type, the CNNs sometimes failed to properly segment the veins. In those cases ($N = 25$), we manually hand-traced the venation network using GIMP. As our CNNs were not trained to segment fossil images, all leaf fossil samples were carefully hand-traced in GIMP by a trained expert. All tracings were error-checked by at least two other experts before finalization. There is some remaining uncertainty in the accuracy of tracings due to the low resolution of some fossil images or imperfect preservation of fossil samples. These issues primarily affect the smaller veins.

The segmentation process resulted in over 19 million veins segmented and resolved veins with width ≥10 µm. All segmented venation networks were then processed in the LeafVeinCNN program to (1) produce a spatial graph representation of the entire venation network (that is, to convert a binary image into a spatial graph where veins are represented by segments of known length and width connected to each other by nodes), (2) generate hierarchical loop decompositions[26,59] (that is, to map a loopy network to a binary tree by sequentially fusing and deleting looping veins of similar diameter) and (3) calculate a series of multiscale venation statistics that describe how the venation network topology and geometry change across vein sizes. Here we focused on four multiscale traits (Fig. 2): VD, MST, ER and CR. VD was calculated as the ratio between all vein segments (in mm) and the one-sided leaf total area (in mm^2). MST was calculated by computing the length of the minimum spanning tree (that is, tree that connects all the vein junctions, without creating any loops and with the minimum possible total length) divided by the length of all veins. ER was calculated by fitting an ellipse to each loop and dividing the major axis length by the minor axis length, then taking the median ratio across all loops. CR was calculated by dividing the loop area by the squared loop perimeter for each loop, then multiplying by 4π, then taking the median value across all loops. To minimize undersampling biases of large veins, we truncated those four multiscale statistics to the 0.01–1.5 mm range of vein width, although larger veins were present (Supplementary Fig. 4). Although those four venation traits have been identified as key traits to capture leading axes of variation in network architecture across many species[3,60], we recognize that other network single-scale (for example, branching angles and connectivity), cross-scale (for example, tapering of veins) and qualitative metrics (for example, pinnate versus palmate) could be important to fully characterize the diversity of architectural designs.

Identifying evolutionary trends in venation traits

We investigated how VD, MST, ER and CR varied over time at each vein spatial scale (small, medium and large sizes). To make an interpretable assessment of trait evolution at different vein spatial scales, we binned vein trait values for each species at three size classes. Because the range of vein widths largely vary across leaf samples (that is, a vein with 0.3 mm width can be a primary vein in a small leaf but a tertiary vein in a large leaf) and some samples show vein tapering (that is, veins become gradually smaller), there was no easy way to use machine-classifiable algorithms to assign each segmented vein to a specific vein order (for example, primary, secondary and tertiary vein classes). Thus, instead of using vein orders, we classified vein widths into three size classes based on their relative sizes (Extended Data Fig. 2). Therefore, our study prioritized greater taxonomic and whole-leaf coverage at the expense of developmental precision in vein classification. To classify

veins into vein size classes, we first standardized (*z*-transformed) vein width values for each species by dividing each vein width by the maximum width value of that species. Therefore, scaled vein sizes varied between 0 and 1 across all species. Next, for each species we classified vein sizes into small (0 < scaled vein width ≤ 0.3), medium (0.3 < scaled vein width ≤ 0.6) and large (scaled vein width > 0.6 mm) classes.

We used the RRphylo R package[16] to investigate the rates and trajectories of diversification over time in each of our four architecture traits at each vein size. RRphylo performs a phylogenetic ridge regression (a maximum-likelihood method) on a phylogenetic tree and associated trait data to return both the ancestral estimates at internal nodes and the branch-wise rates of trait evolution[61]. Those rates are phylogenetic ridge regression coefficients (that is, represent the trait change per unit time between consecutive nodes in the tree), so they have both a direction (indicating whether the mean trait value increases or decreases over time) and a magnitude (indicating the speed of mean trait value change over time). RRphylo assumes no specific a priori evolutionary model about the tempo and mode of trait evolution. It is also specifically designed to process phylogenies including fossil species (that is, fossil trait information is directly integrated in the ancestral state reconstruction), which improves, and in some cases even changes, our understanding of trait evolution[60].

To test for the existence of evolutionary trends (that is, directional patterns of evolutionary trait mean change over time) in venation architecture, we applied the function 'search.trend' from RRphylo for each trait at each vein class. This function first performs a linear phylogenetic ridge regression between trait values (obtained by collating ancestral state estimates to measured trait values at the tree tips) and evolutionary rates (trait change per unit time between consecutive nodes in the tree) versus ages (their distance from the tree root). A potential limitation of this approach is that only linear associations are considered; that is, nonlinear trends in single traits were not examined here. Significance of the linear evolutionary trends was assessed as the probability that those linear regression slopes differ from a family of 100 regression slopes ('BMslopes') generated according to the Brownian motion (BM) model of evolution. In the BM simulations, species mean trait values are assumed to evolve through a flat adaptive landscape, that is, the evolutionary changes along branches in the tree have an expected value of zero and are normally distributed with a variance proportional to the length of the branch. A significant evolutionary trend exists whenever the trait regression slopes significantly depart from the BMslopes simulations. Therefore, for a two-tailed test at $\alpha = 0.05$, significant trends exist whenever p.random < 0.05 (significant decrease in rates or trait means over time) or p.random > 0.95 (significant increase). The search.trend function was used to identify evolutionary trends both on vascular plants as a whole (that is, for the entire plant phylogeny) and on each focal clade individually. In the latter case, clades presumed to experience trended evolution must be indicated by their nodes. Because in our tree the clade basal eudicots constitute a paraphyletic group (Fig. 1), we ran search.trend function separately for the orders Ranunculales (basal eudicots 1), Proteales (basal eudicots 2) and Saxifragales (basal eudicots 3). Following recent analysis based on nuclear data[62], we placed the orders Santalales, Berberidopsidales and Caryophyllales in the asterid clade ('superasterids'). All *P* values generated using the search.trend function were adjusted using the Benjamini and Hochberg[63] correction, as implemented in the R function 'p.adjust'.

To assess whether the evolutionary trends identified were robust to sampling and phylogenetic uncertainty, we applied the overfitRR function from the RRphylo R package[58]. This function randomly removes a number of species corresponding to approximately 25% of the tree size, swaps the phylogenetic position of approximately 15% of tips (tips are swapped across up to two nodes) and 'moves' in time 15% of the tree nodes (nodes are changed in age between the age of its ancestor and the age of its daughter node). Then, it performs search.trend on the new tree and data. This procedure is repeated 100 times, and the percentage of significant results is returned. The overfitRR function also regresses the original ancestral reconstructed states at internal nodes with the states produced after each subsampling and swapping. Regression slopes close to 1 indicate a closer match between original and resampled values, suggesting more robust estimation[58].

To test for statistically significant differences among the venation traits evolutionary rates across vein sizes, we used Wilcoxon tests, as implemented in the R package 'rstatix'. To facilitate comparisons across vein sizes and across different venation traits, Wilcoxon tests were conducted on the absolute log-transformed evolutionary rates obtained with the RRphylo approach described in the section above.

Disparity through time analysis

To investigate in which clades the evolution of novel architectural trait combinations have originated and how the diversity of architectures varied over time, we performed a disparity (multidimensional space occupancy) analysis using the 'dispRity' R package[64]. First, we carried out a PCA across the four venation traits at each vein class to define the multidimensional venation architectural space (morphospace). PCA was run by collating ancestral state estimates at internal nodes to trait values measured at the tree tips. Before PCA, all traits were centred and scaled (*z*-transformed) to improve comparability among them and to reduce bias towards traits with higher variance. VD and ER values were also square-root-transformed to improve normality. Using this 12-dimensional architectural space, we calculated two metrics of disparity describing complementary aspects of the multidimensional space occupancy: (1) the median centroids—equation (1), the median distance between each element and the centroid of the ordinated space, which describes the position of an element in the morphospace compared to a fixed point in this space (that is, the space centroid); and (2) the sum variances—equation (2), the sum of variance of each dimension of the ordinated space, which characterizes the size of morphospace occupied by each element[63].

$$\text{Centroids} = \sqrt{\sum_{i=1}^{n}\left(d_n - \text{centroid}_d\right)^2} \quad (1)$$

$$\text{Variances} = \sigma^2 d_i \quad (2)$$

where d is the number of dimensions, n is the number of elements, σ^2 is the variance of each dimension and i is any row of the data.

To test whether different clades occupy different regions of the architectural space, we used the function 'dispRity.per.group', which measured the disparity between each clade. To make each time slice more robust to outliers, we used the 'boot.matrix' function which pseudo-replicate the (PCA) ordination matrix used for the disparity measurements 100 times to see how sensitive they are to outliers in the dataset. Significant differences in morphospace occupation among clades were then tested using the 'test.dispRity' function, which performed a nonparametric multivariate analysis of variance followed by post hoc *t*-test with Bonferroni *P*-value correction.

To test how the space occupancy varied across time (for example, test whether the disparity metrics increased or decreased over time), we used the 'dispRity.through.time' function[64] to conduct a disparity-through-time (DTT) analyses using the time-slicing method[65]. Unlike other DTT methods based on time binning, time slicing (continuous time subsets) uses a time-calibrated phylogenetic tree and considers subsets of taxa at specific equidistant points in time, which results in even sampling across time and allows the definition of the underlying model of character evolution (punctuated or gradual evolution). As we did not have an a priori hypothesis for the model of venation architecture evolution, we performed the time slicing using two alternative models: a punctuated model (that is, 'proximity') and a gradual model (that is, 'gradual.splits') of evolution[65]. Those model

arguments (proximity or gradual.splits) are used when the time slice occurs along a branch of the tree rather than on a tip or a node, meaning that a decision must be made about what the value for the branch should be. In both time-slicing models, we divided the approximately 400 million year time frame of vascular plant evolution into 40 time slices of approximately 10 Myr duration each. Extant taxa were split inside each time slice according to their age (taxa were considered as single points in time). To account for the uncertainty in the fossil ages, the first and last occurrence data for each fossil taxon were used during the time-slicing process, so those taxa could appear in more than one time slice. To make each time slice more robust to outliers, we used the boot.matrix function to perform 100 bootstrapping iterations in the PCA dataset. Next, we used the function test.dispRity to test for significant changes in disparity over time using Wilcoxon test applied to time sliced disparity with sequential comparisons and Bonferroni *P* value correction. DTT analysis was performed both for the entire dataset (all 1,000 species together) and for each clade separately. In the latter case, we first used the function 'extract.clade' from the 'ape' R package to extract a subtree for each clade, then we conducted the DTT analysis on each of those subtrees. The number of time slices used varied among clades and was determined by dividing the root tree age by 10, so for all clades each time slice had a fixed duration of approximately 10 Myr.

Finally, we also quantified the evolutionary mode of venation architecture diversification by using the 'model.test' function to fit five alternative modes of disparity changes through time: (1) stasis (time-invariant change, null expectation of time-invariant change in disparity in which disparity values fluctuate with a variance around the mean); (2) Brownian-motion model (BM—random-walk, assumes a constant mean that is equal to the ancestral estimate of the sequence, and the variance around this mean increases linearly with time); (3) Ornstein–Uhlenbeck (OU—evolution constrained to an optima); (4) trend (increasing or decreasing mean through time); and (5) early burst (EB—exponentially decreasing rate through time). The goodness of fit of each candidate evolutionary model was then determined using Akaike information criterion (AIC) scores, and the model with lowest AIC was selected as the best.

Associations between venation and biotic and abiotic proxies

To explore abiotic and biotic factors that may have influenced leaf venation evolution in vascular plants, we compared the reconstructed evolutionary trajectories of single venation traits and the patterns of venation architectural disparity with global average temperature[17], atmospheric CO_2 concentration[18] and global insect diversification rates[19] for the Phanerozoic eon. In the absence of global insect diversification rates for phytophagous versus non-phytophagous insects, we assumed those rates to be consistent with each other, as for the majority of insect orders a strong and positive relationship exists between herbivory and diversification rates[40]. Time-binned median values of each of these time-series data sets were calculated (at ~10 Myr bins for the pooled regressions or at ~2 Myr bins for the individual clade regressions) and used in the regression analyses. To test for temporal autocorrelation in our datasets, we first ran multivariate ordinary least squares regressions between each response variable (VD_{small}, VD_{medium}, CR_{small}, CR_{medium}, MST_{small}, MST_{medium}, sum of variances and median of centroids) and all our predictor variables (CO_2, temperature and insect rates), for example, VD_{small} ~CO_2 + temperature + insect rates. Then, we used the Durbin–Watson test to check for significant autocorrelation in the residuals of the ordinary least squares regressions. Whenever this test was significant ($P < 0.05$), we refit the model using GLS regression fitted by maximizing the restricted log-likelihood (REML) with an autocorrelation moving-average structure of order one to three (for example, VD_{small} ~CO_2 + temperature + insect rates, correlation = corARMA ($p = n$), method = 'REML'; where $n = 1$, 2 or 3) as implemented in the R package 'nlme'. This approach estimates the strength of serial correlation in the relationship between variables, correcting for the non-independence of adjacent points within a time series. Finally, we chose the GLS model with best fit according to the AIC. To test for potential interactive effects between abiotic variables, we also ran additional models including an interaction term between CO_2 and temperature (for example, VD_{small} ~CO_2 × temperature + insect diversification rates) for all species pooled together. Additional regression analyses, using only angiosperm species, were run to investigate potential compensatory effects of the presence of leaf exudates (that is, resins and latex) on the correlation between insect diversification rates and venation traits (Supplementary Note 2). Note that we only ran those time-series regression analysis for the venation traits and clades that had shown a significant evolutionary trend in accordance with the analysis described in the two sections above.

All analyses were carried out using R version 4.3.1 (R Core Team, 2023).

Reporting summary

Further information on research design is available in the Nature Portfolio Reporting Summary linked to this article.

Data availability

The data needed to reproduce all analyses are publicly available on Zenodo at https://doi.org/10.5281/zenodo.13300782 (ref. 66). The original cleared leaf images, leaf masks, extracted networks and all LeafVeinCNN outputs for the 122 leaf samples collected at the UCBG at Berkeley are available on Dryad at https://doi.org/10.5061/dryad.1g1jwsv36 (ref. 67). Network segmentations and leaf masks of all other 878 samples are available on Zenodo at https://doi.org/10.5281/zenodo.13300782 (ref. 66) and https://doi.org/10.5281/zenodo.15217651 (ref. 68). These three previous datasets also contain high-resolution cleared leaf images from Ecuador, Costa Rica, Ghana and UCMP collections. Original leaf cleared images of all other extant species are available via Wilf collection at https://phytokeys.pensoft.net/article/72350/ and Smithsonian National Cleared Leaf Collection at https://collections.peabody.yale.edu/pb/nclc/. Original fossil leaf images are publicly available at https://peabody.yale.edu/, www.gbif.org, https://www.museumfuernaturkunde.berlin/, https://ucmpdb.berkeley.edu/, https://www.floridamuseum.ufl.edu/, https://search.museums.ualberta.ca/, https://ucmp.berkeley.edu/collections/paleobotany-collection/, https://phytokeys.pensoft.net/article/72350/, https://doi.org/10.1016/j.palwor.2017.01.003, https://doi.org/10.1080/14772019.2014.936974, https://doi.org/10.1080/11035890902857846, https://doi.org/10.1016/j.revpalbo.2009.08.004, https://doi.org/10.1016/j.revpalbo.2017.08.003, https://doi.org/10.1515/acpa-2017-0012 and https://api.semanticscholar.org/CorpusID:135128574. World Plants (https://worldplants.de/), Paleobiology (https://paleobiodb.org/) and Fossilworks (fossilworks.org) databases were used to standardize species names. TimeTree: the timescale of life (https://timetree.org/) database was used to recalibrate the age of internal nodes of the phylogenetic tree.

Code availability

The R code needed to reproduce all analyses and figures is publicly available on Zenodo at https://doi.org/10.5281/zenodo.13300782 (ref. 66).

References

1. Boyce, C. K., Brodribb, T. J., Feild, T. S. & Zwieniecki, M. A. Angiosperm leaf vein evolution was physiologically and environmentally transformative. *Proc. R. Soc. B* **276**, 1771–1776 (2009).
2. Sack, L. & Scoffoni, C. Leaf venation: structure, function, development, evolution, ecology and applications in the past, present and future. *New Phytol.* **198**, 983–1000 (2013).

3. Blonder, B. et al. Linking functional traits to multiscale statistics of leaf venation networks. *New Phytol.* **228**, 1796–1810 (2020).
4. Matos, I. S. et al. Leaf venation network architecture coordinates functional trade-offs across vein spatial scales: evidence for multiple alternative designs. *New Phytol.* **7244**, 407–425 (2024). nph.2003.
5. Bres, J., Sepulchre, P., Viovy, N. & Vuichard, N. The Cretaceous physiological adaptation of angiosperms to a declining pCO_2: a modeling approach emulating paleo-traits. *Biogeosciences* https://doi.org/10.5194/bg-2021-139 (2021).
6. Beerling, D. J. Leaf evolution: gases, genes and geochemistry. *Ann. Bot.* **96**, 345–352 (2005).
7. Brodribb, T. J. & Feild, T. S. Leaf hydraulic evolution led a surge in leaf photosynthetic capacity during early angiosperm diversification. *Ecol. Lett.* **13**, 175–183 (2010).
8. Feild, T. S. et al. Fossil evidence for Cretaceous escalation in angiosperm leaf vein evolution. *Proc. Natl Acad. Sci. USA* **108**, 8363–8366 (2011).
9. Boyce, C. K. & Knoll, A. H. Evolution of developmental potential and the multiple independent origins of leaves in Paleozoic vascular plants. *Paleobiology* **28**, 70–100 (2002).
10. Boyce, C. K. Patterns of segregation and convergence in the evolution of fern and seed plant leaf morphologies. *Paleobiology* **31**, 117–140 (2005).
11. Walls, R. L. Angiosperm leaf vein patterns are linked to leaf functions in a global-scale data set. *Am. J. Bot.* **98**, 244–253 (2011).
12. Kawai, K. & Okada, N. Roles of major and minor vein in leaf water deficit tolerance and structural properties in 11 temperate deciduous woody species. *Trees* **32**, 1573–1582 (2018).
13. Kawai, K. & Okada, N. How are leaf mechanical properties and water-use traits coordinated by vein traits? A case study in Fagaceae. *Funct. Ecol.* **30**, 527–536 (2016).
14. Katifori, E., Szöllősi, G. J. & Magnasco, M. O. Damage and fluctuations induce loops in optimal transport networks. *Phys. Rev. Lett.* **104**, 048704 (2010).
15. Benton, M. J., Wilf, P. & Sauquet, H. The Angiosperm Terrestrial Revolution and the origins of modern biodiversity. *New Phytol.* **233**, 2017–2035 (2022).
16. Castiglione, S. et al. A new method for testing evolutionary rate variation and shifts in phenotypic evolution. *Methods Ecol. Evol.* **9**, 974–983 (2018).
17. Scotese, C. R., Song, H., Mills, B. J. W. & Van Der Meer, D. G. Phanerozoic paleotemperatures: the earth's changing climate during the last 540 million years. *Earth Sci. Rev.* **215**, 103503 (2021).
18. Foster, G. L., Royer, D. L. & Lunt, D. J. Future climate forcing potentially without precedent in the last 420 million years. *Nat. Commun.* **8**, 14845 (2017).
19. Condamine, F. L., Clapham, M. E. & Kergoat, G. J. Global patterns of insect diversification: towards a reconciliation of fossil and molecular evidence? *Sci. Rep.* **6**, 19208 (2016).
20. Castiglione, S., Serio, C., Mondanaro, A., Melchionna, M. & Raia, P. Fast production of large, time-calibrated, informal supertrees with tree.merger. *Palaeontology* **65**, e12588 (2022).
21. Sack, L. et al. Developmentally based scaling of leaf venation architecture explains global ecological patterns. *Nat. Commun.* **3**, 837 (2012).
22. De Boer, H. J., Eppinga, M. B., Wassen, M. J. & Dekker, S. C. A critical transition in leaf evolution facilitated the Cretaceous angiosperm revolution. *Nat. Commun.* **3**, 1221 (2012).
23. Brodribb, T. J., Feild, T. S. & Sack, L. Viewing leaf structure and evolution from a hydraulic perspective. *Funct. Plant Biol.* **37**, 488 (2010).
24. Blonder, B., Violle, C., Bentley, L. P. & Enquist, B. J. Venation networks and the origin of the leaf economics spectrum. *Ecol. Lett.* **14**, 91–100 (2011).
25. Silvestro, D., Cascales-Miñana, B., Bacon, C. D. & Antonelli, A. Revisiting the origin and diversification of vascular plants through a comprehensive Bayesian analysis of the fossil record. *New Phytol.* **207**, 425–436 (2015).
26. Katifori, E. & Magnasco, M. O. Quantifying loopy network architectures. *PLoS ONE* **7**, e37994 (2012).
27. Brodribb, T. J., Feild, T. S. & Jordan, G. J. Leaf maximum photosynthetic rate and venation are linked by hydraulics. *Plant Physiol.* **144**, 1890–1898 (2007).
28. Niklas, K. J. Morphological evolution through complex domains of fitness. *Proc. Natl Acad. Sci. USA* **91**, 6772–6779 (1994).
29. Boyce, C. K. & Leslie, A. B. The paleontological context of angiosperm vegetative evolution. *Int. J. Plant Sci.* **173**, 561–568 (2012).
30. Ramírez-Barahona, S., Sauquet, H. & Magallón, S. The delayed and geographically heterogeneous diversification of flowering plant families. *Nat. Ecol. Evol.* **4**, 1232–1238 (2020).
31. Blonder, B., Royer, D. L., Johnson, K. R., Miller, I. & Enquist, B. J. Plant ecological strategies shift across the Cretaceous–Paleogene boundary. *PLoS Biol.* **12**, e1001949 (2014).
32. Sperry, J. S., Hacke, U. G., Feild, T. S., Sano, Y. & Sikkema, E. H. Hydraulic consequences of vessel evolution in angiosperms. *Int. J. Plant Sci.* **168**, 1127–1139 (2007).
33. Feild, T. S. & Wilson, J. P. Evolutionary voyage of angiosperm vessel structure-function and its significance for early angiosperm success. *Int. J. Plant Sci.* **173**, 596–609 (2012).
34. Ueno, O., Kawano, Y., Wakayama, M. & Takeda, T. Leaf vascular systems in C3 and C4 grasses: a two-dimensional analysis. *Ann. Bot.* **97**, 611–621 (2006).
35. Hughes, M., Gerber, S. & Wills, M. A. Clades reach highest morphological disparity early in their evolution. *Proc. Natl Acad. Sci. USA* **110**, 13875–13879 (2013).
36. Oyston, J. W., Hughes, M., Gerber, S. & Wills, M. A. Why should we investigate the morphological disparity of plant clades? *Ann. Bot.* **117**, 859–879 (2016).
37. Beerling, D. J. & Berner, R. A. Feedbacks and the coevolution of plants and atmospheric CO_2. *Proc. Natl Acad. Sci. USA* **102**, 1302–1305 (2005).
38. Labandeira, C. C. & Currano, E. D. The fossil record of plant-insect dynamics. *Annu. Rev. Earth Planet. Sci.* **41**, 287–311 (2013).
39. Coley, P. D. & Barone, J. A. Herbivory and plant defenses in tropical forests. *Annu. Rev. Ecol. Syst.* **27**, 305–335 (1996).
40. Wiens, J. J., Lapoint, R. T. & Whiteman, N. K. Herbivory increases diversification across insect clades. *Nat. Commun.* **6**, 8370 (2015).
41. Rashid War, A. et al. Plant defense against herbivory and insect adaptations. *AoB Plants* https://doi.org/10.1093/aobpla/ply037 (2018).
42. Wilf, P. et al. An image dataset of cleared, X-rayed, and fossil leaves vetted to plant family for human and machine learning. *PhytoKeys* **187**, 93–128 (2021).
43. Matos, I. S. et al. Leaf architecture and functional traits for 122 species at the University of California Botanical Garden at Berkeley. *Ecology* **105**, e4436 (2024).
44. Niewiadomski, I. et al. A comprehensive illustrated protocol for clearing, mounting, and imaging leaf venation networks. *Appl. Plant Sci.* **13**, e70002 (2025).
45. Deng, S.-H. et al. Plant fossils from the Lower Jurassic coal-bearing formation of central Inner Mongolia of China and their implications for palaeoclimate. *Palaeoworld* **26**, 279–316 (2017).
46. Escapa, I. H., Bomfleur, B., Cuneo, N. R. & Scasso, R. A new marattiaceous fern from the Lower Jurassic of Patagonia (Argentina): the renaissance of *Marattiopsis*. *J. Syst. Palaeontol.* **13**, 677–689 (2015).

47. McLoughlin, S. & Pott, C. The Jurassic flora of Western Australia. *GFF* **131**, 113–136 (2009).
48. Pott, C. & McLoughlin, S. Bennettitalean foliage in the Rhaetian–Bajocian (latest Triassic–Middle Jurassic) floras of Scania, southern Sweden. *Rev. Palaeobot. Palynol.* **158**, 117–166 (2009).
49. Na, Y. et al. A brief introduction to the Middle Jurassic Daohugou flora from Inner Mongolia, China. *Rev. Palaeobot. Palynol.* **247**, 53–67 (2017).
50. Pott, C. & Jiang, B. Plant remains from the Middle–Late Jurassic Daohugou site of the Yanliao Biota in Inner Mongolia, China. *Acta Palaeobot.* **57**, 185–222 (2017).
51. Scanu, G. G., Kustatscher, E. & Pittau, P. The Jurassic plant fossils of the Lovisato Collection: preliminary notes. *Boll. Soc. Paleontol. Ital.* **51**, 71–84 (2012).
52. McElwain, J. C., Yiotis, C. & Lawson, T. Using modern plant trait relationships between observed and theoretical maximum stomatal conductance and vein density to examine patterns of plant macroevolution. *New Phytol.* **209**, 94–103 (2016).
53. Zhang, J. & Qian, H. U. Taxonstand: an R package for standardizing scientific names of plants and animals. *Plant Divers.* **45**, 1–5 (2023).
54. The Angiosperm Phylogeny Group. An update of the Angiosperm Phylogeny Group classification for the orders and families of flowering plants: APG IV. *Bot. J. Linn. Soc.* **181**, 1–20 (2016).
55. Jin, Y. & Qian, H. V.PhyloMaker2: an updated and enlarged R package that can generate very large phylogenies for vascular plants. *Plant Divers.* **44**, 335–339 (2022).
56. Kumar, S., Stecher, G., Suleski, M. & Hedges, S. B. TimeTree: a resource for timelines, timetrees, and divergence times. *Mol. Biol. Evol.* **34**, 1812–1819 (2017).
57. Cleal, C. J. & Shute, C. H. The systematic and palaeoecological value of foliage anatomy in Late Palaeozoic medullosalean seed-plants. *J. Syst. Palaeontol.* **10**, 765–800 (2012).
58. Serio, C. et al. Macroevolution of toothed whales exceptional relative brain size. *Evol. Biol.* **46**, 332–342 (2019).
59. Xu, H., Blonder, B., Jodra, M., Malhi, Y. & Fricker, M. Automated and accurate segmentation of leaf venation networks via deep learning. *New Phytol.* **229**, 631–648 (2021).
60. Blonder, B. et al. Structural and defensive roles of angiosperm leaf venation network reticulation across an Andes–Amazon elevation gradient. *J. Ecol.* **106**, 1683–1699 (2018).
61. Castiglione, S. et al. Simultaneous detection of macroevolutionary patterns in phenotypic means and rate of change with and within phylogenetic trees including extinct species. *PLoS ONE* **14**, e0210101 (2019).
62. Zuntini, A. R. et al. Phylogenomics and the rise of the angiosperms. *Nature* **629**, 843–850 (2024).
63. Benjamini, Y. & Hochberg, Y. Controlling the false discovery rate: a practical and powerful approach to multiple testing. *J. R. Stat. Soc. B* **57**, 289–300 (1995).
64. Guillerme, T. dispRity: a modular R package for measuring disparity. *Methods Ecol. Evol.* **9**, 1755–1763 (2018).
65. Guillerme, T. & Cooper, N. Time for a rethink: time sub-sampling methods in disparity-through-time analyses. *Palaeontology* **61**, 481–493 (2018).
66. Matos, I. S., et al. Macroevolutionary trends in leaf venation network architecture. *Zenodo* https://doi.org/10.5281/zenodo.13300782 (2025).
67. Matos, I., et al. Leaf architecture and functional traits for 122 species at the University of California at Berkeley botanical garden. *Dryad* https://doi.org/10.5061/dryad.1g1jwsv36 (2024).
68. Boakye, M., et al. Leaf venation network architectural traits along a forest-savannah gradient in Ghana. *Zenodo* https://doi.org/10.5281/zenodo.15217651 (2025).

Acknowledgements

This study was supported by the US National Science Foundation (grant DEB-2025282, B.B.) with supplements from the Research Experience for Undergraduates, Research Experience for Post-Baccalaureate Students and Research Experience for Teachers programs, the University of California at Berkeley Sponsored Projects for Undergraduate Research program, and the UK Natural Environment Research Council (NE/M019160/1, M.F.). Ghana samples were collected under permit of the Forestry Research Institute of Ghana (FORIG, M.B.) at Kumasi, Ghana. Costa Rica samples were collected under permit ACOPAC-INV-RES-002-11, issued to B.B. by the Ministerio de Ambiente, Energía y Telecomunicaciones, Área de Conservación del Pacífico Central. Ecuador samples were collected under Ministerio Del Ambiente permit 004-2019-IC-PNY-DPAO/AVS and exported under permit MAE-DPAO-2019-1275-O. Ecuador field sampling efforts were funded by CTFS ForestGeo grants program and the Arizona State University WAESO program, which funded the undergraduate research technicians that processed the Ecuador leaf samples. We acknowledge P. Wilf for organizing and publishing a large image database of extant cleared and fossil leaves and thank him for providing useful feedback on a first draft of this paper. We thank S. Castiglione and P. Raia for providing input on RRphylo, and S. Rifai for providing computational support for the bootstrapping analysis. We are grateful to all staff of the UCBG at Berkeley for the logistical support, especially to the horticulturists E. Fenner, E. Hupperts, J. Fong, N. Gapsis, G. Dollarhide, S. Warsh, J. Bonham and C. Rieder, who helped us with sample collection.

Author contributions

B.W.B., M.F., L.M.T.A. and B.J.E. acquired funding. I.S.M. and B.W.B. designed the study. M.F. developed the program for leaf venation extraction, which was improved by B.W.B., S.S., S.M. and C.T., using venation images hand-traced by C.P., N.V. and H.J.P. H.F. and D.M.E. provided logistical support to access the UCBG living collections and the UCMP cleared leaf collections, respectively. I.N. led a lab team group responsible for clearing (S.C., M.A., A.C., M.S., N.Y.) and imaging (A.E.) the UCBG leaf samples. L.M.T.A., E.G.H., R.E.C., M.R. and M.A.D. collected and prepared the Ecuador leaf samples. M.B. collected the Ghana leaf samples. B.B. collected the Costa Rica leaf samples with funding from B.J.E. E.G.H. collected the Ecuador leaf samples with funding from L.M.T.A. E.X. selected and imaged the UCMP leaf samples. B.V., J.M., N.V., M.B., I.S.M. and C.P. hand-traced leaf images and prepared leaf masks of extant species, while M.B.F., R.J.W. and J.L. hand-traced fossil leaf images. B.V., J.M., M.S. and I.S.M. used the LeafVeinCNN program to extract the leaf venation networks and the leaf architectural traits. K.D. provided critical support for the data analysis. I.S.M. analysed the data and drafted the paper. All authors contributed to and revised the paper.

Competing interests

The authors declare no competing interests.

Additional information

Extended data is available for this paper at https://doi.org/10.1038/s41477-025-02011-y.

Supplementary information The online version contains supplementary material available at https://doi.org/10.1038/s41477-025-02011-y.

Correspondence and requests for materials should be addressed to Ilaine Silveira Matos.

Peer review information *Nature Plants* thanks Christopher Baraloto and the other, anonymous, reviewer(s) for their contribution to the peer review of this work.

[1]Department of Environmental Science, Policy, and Management, University of California Berkeley, Berkeley, CA, USA. [2]School of Biological Sciences, The University of Adelaide, Adelaide, South Australia, Australia. [3]Division of Infectious Diseases and Geographic Medicine, Department of Medicine, Stanford University, Stanford, CA, USA. [4]Department of Biology, University of Waterloo, Waterloo, Ontario, Canada. [5]School of Life Sciences, Arizona State University, Tempe, AZ, USA. [6]School of Biological Sciences, The University of Utah, Salt Lake City, UT, USA. [7]Escuela de Ciencias Biológicas, Pontificia Universidad Católica del Ecuador, Quito, Ecuador. [8]Department of Ecology & Evolutionary Biology, The University of Arizona, Tucson, AZ, USA. [9]Department of Plants & Soil Sciences, University of Delaware, Newark, DE, USA. [10]University of California Museum of Paleontology, Berkeley, CA, USA. [11]University of California Botanical Garden at Berkeley, Berkeley, CA, USA. [12]School of GeoSciences, University of Edinburgh, Edinburgh, UK. [13]Royal Botanic Garden Edinburgh, Edinburgh, UK. [14]Department of Life Sciences and Systems Biology, University of Turin, Turin, Italy. [15]Department of Biology, University of Oxford, Oxford, UK. ✉e-mail: ilaine.matos@gmail.com

https://doi.org/10.1038/s41477-025-02011-y

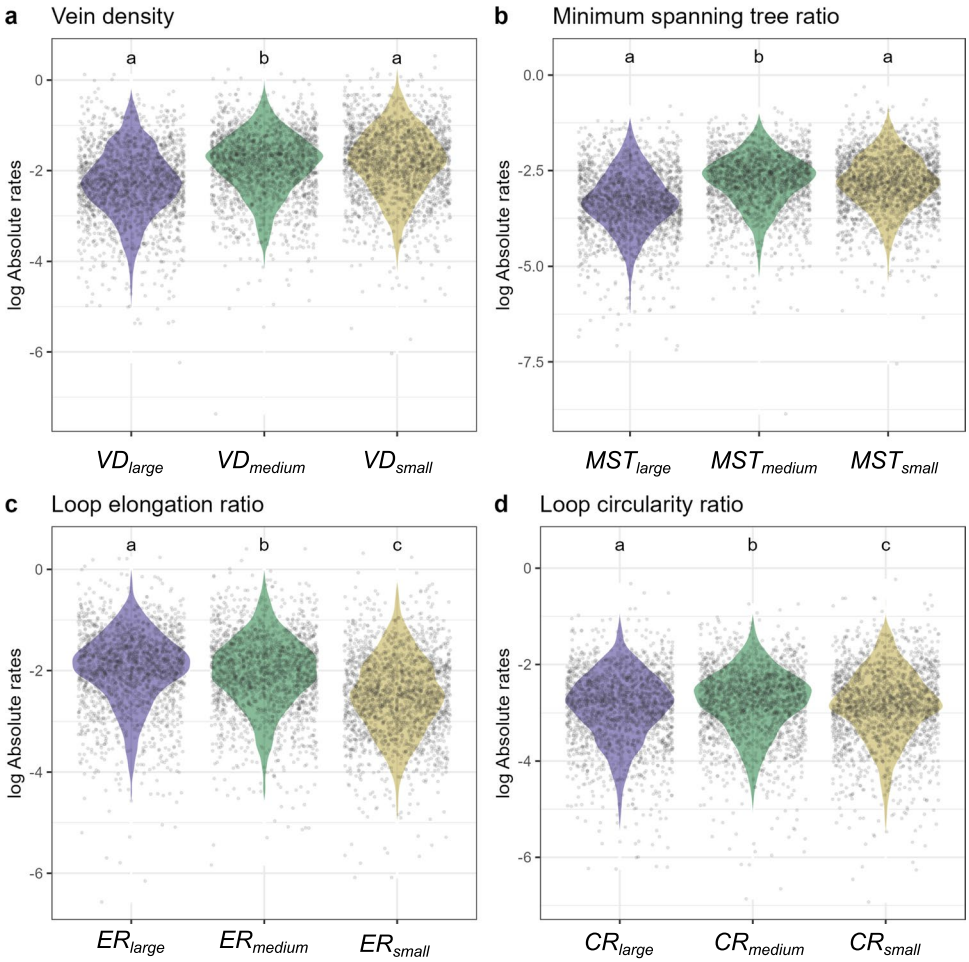

Extended Data Fig. 1 | Evolutionary rates of leaf venation architecture traits across vein sizes. a, Vein density - VD (F: - −0.72; CI: −0.16/0.55; P-value < 0.01); **b**, Minimum spanning tree ratio - MST (F: −1.43; CI: −0.007/1.43; P-value < 0.01); **c**, Loop elongation ratio - ER (F: 0.58; CI: 1.44/0.87; P-value < 0.01); **d**, Loop circularity ratio - CR (F: −1.20; CI: 0.15/1.35; P-value < 0.01). Letters indicate significant differences (p-value < 0.05) in two-sided Wilcoxon signed-rank test followed by Bonferroni p-value correction. Data is presented as median and the Kernel Density Estimation boundary.

https://doi.org/10.1038/s41477-025-02011-y

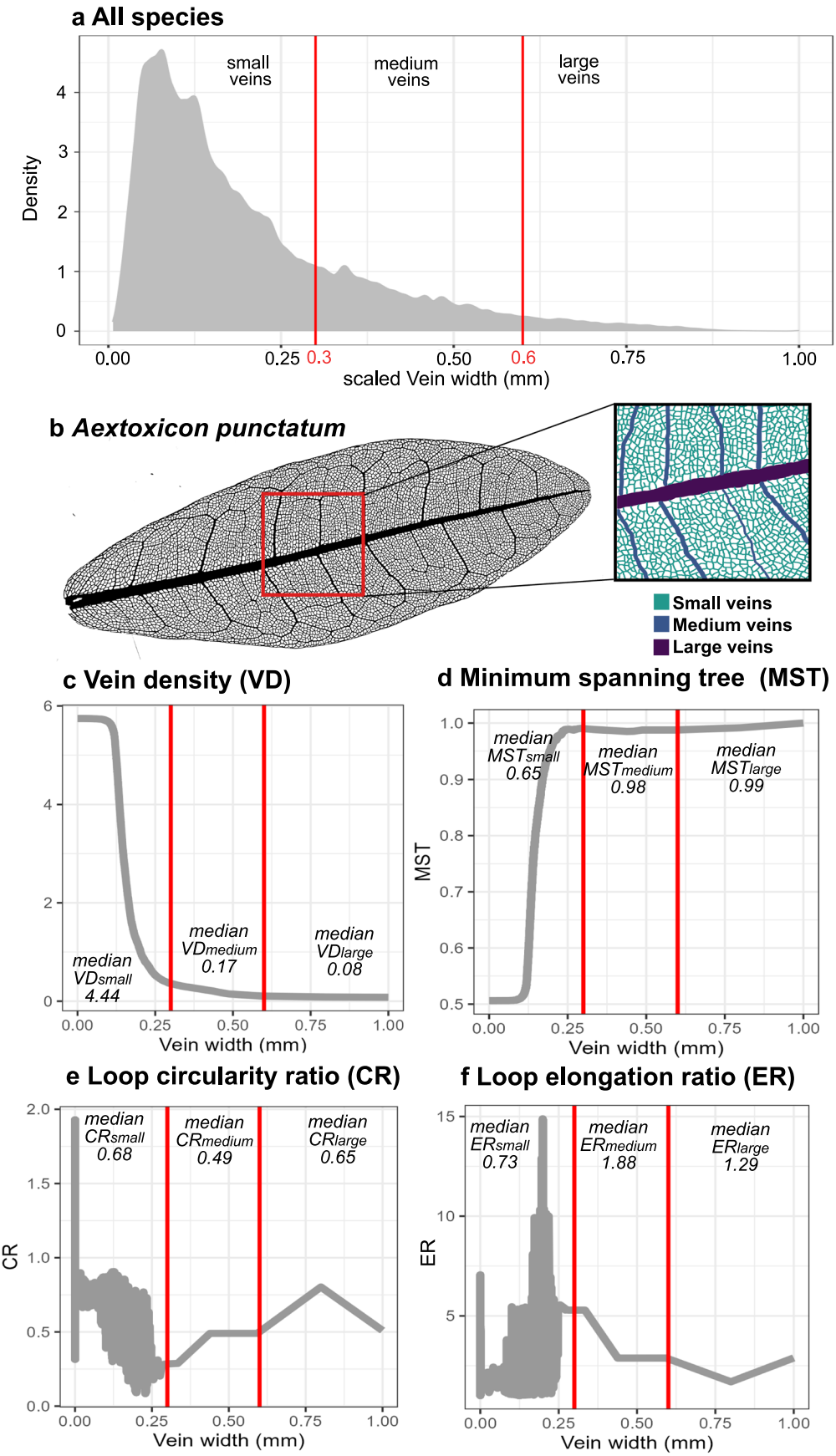

Extended Data Fig. 2 | Classification of veins into three size classes (small, medium, large). (a) Density plot of scaled vein width for all 1,000 species evaluated in this study. The red lines indicate the limits used to define the three vein size classes. **(b)** Detail of the leaf venation network for the species *Aextoxicon punctatum*, showing the small, medium, and large veins. Distribution of **(c)** Vein density (VD), **(d)** Minimum spanning tree ratio (MST), **(e)** Loop circularity ratio (CR), and **(f)** Loop elongation ratio (ER) across vein widths for *A. punctatum*. Panels **d**-**g** show the median values for each venation trait at each vein size class.

https://doi.org/10.1038/s41477-025-02011-y

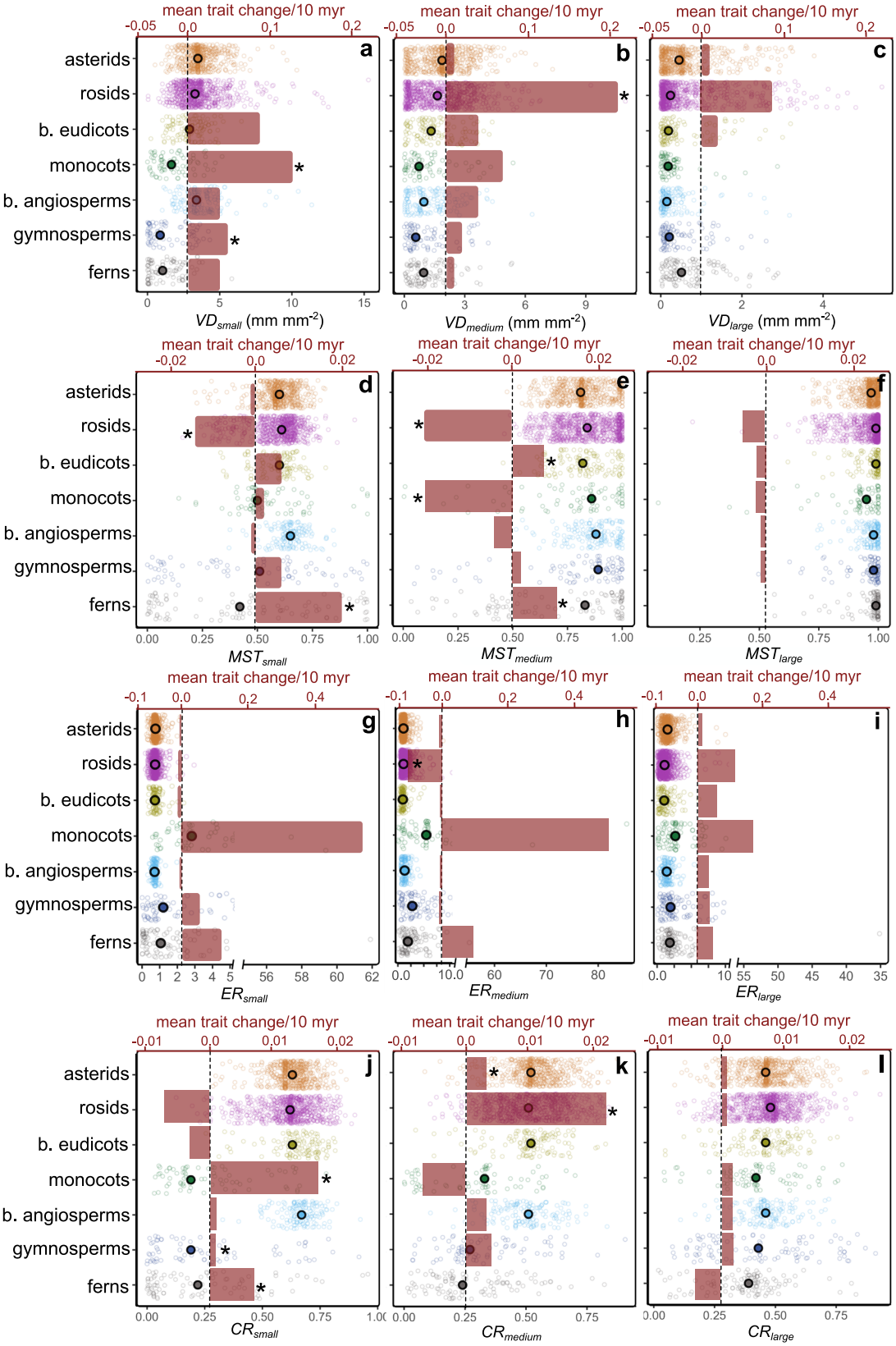

Extended Data Fig. 3 | Evolutionary trends in leaf venation architecture traits across plant clades and vein sizes. a-c, Vein density (*VD*). **d-f**, Minimum spanning tree ratio (*MST*). **g-i**, Loop elongation ratio (*ER*). **j-l**, Loop circularity ratio (*CR*). In each panel the bottom axis and jittered points show the venation trait distribution in each plant clade, with the median value highlighted by the hollow black circle. The top axis and dark red bars show the mean trait evolutionary rate per 10 million years. An '*' indicates a significant linear evolutionary trend (α = 0.05) of increase (positive values) or decrease (negative values) in mean trait values over time according to phylogenetic ridge regressions.

https://doi.org/10.1038/s41477-025-02011-y

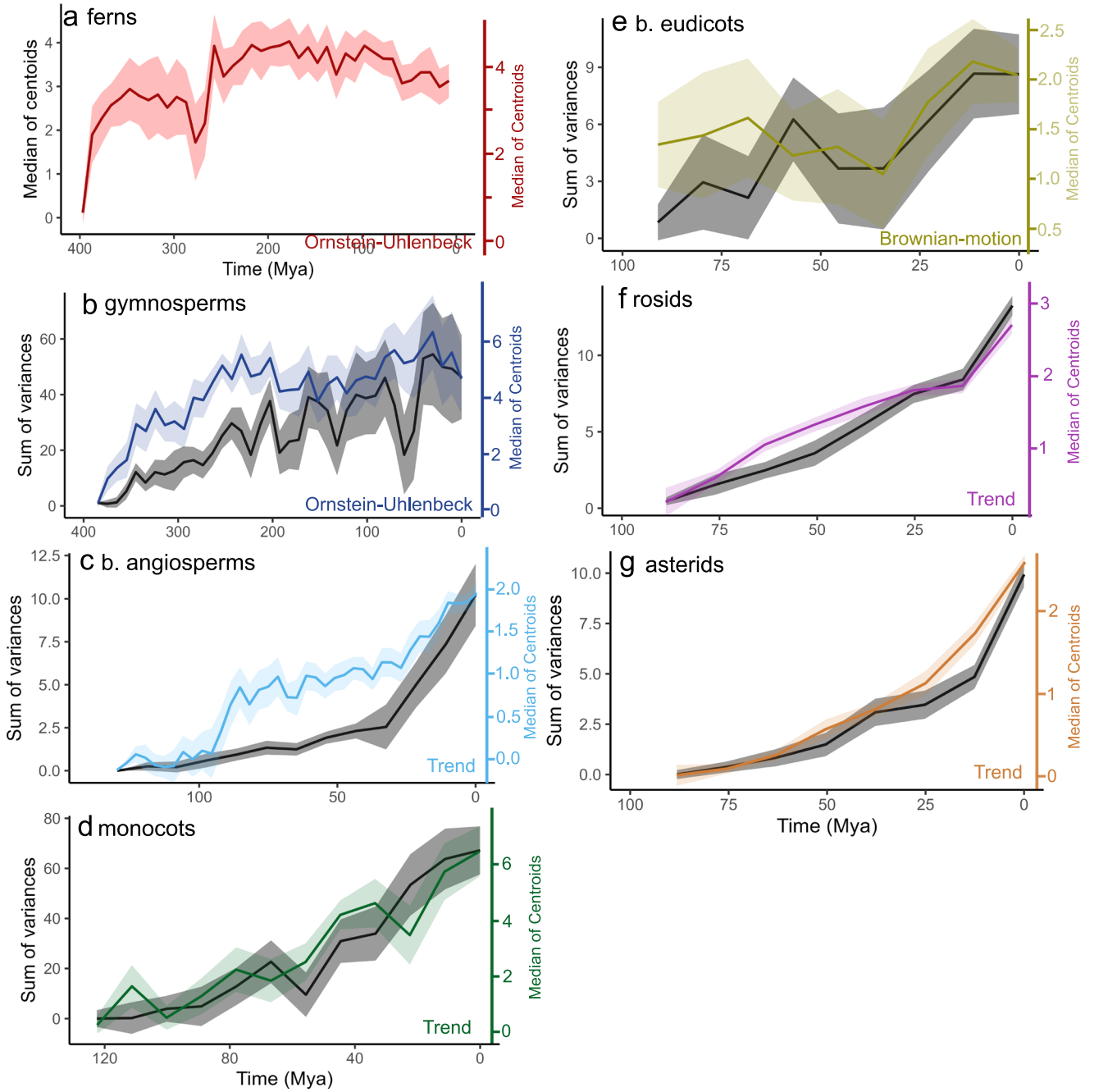

Extended Data Fig. 4 | Results of disparity through time analysis under a gradual model of evolution for each vascular plant clade. a, ferns; **b**, gymnosperms; **c**, basal angiosperms; **d**, monocots; **e**, basal eudicots; **f**, rosids; **g**, asterids. Each panel shows the temporal dynamics of two complementary metrics of disparity, the sum of variances (describing the position occupied in the venation architectural) and the median of centroids (describing the extent of space occupied). Lines represent the median values for each time-slice of ca. 10 million years of duration and the corresponding standard deviation.

https://doi.org/10.1038/s41477-025-02011-y

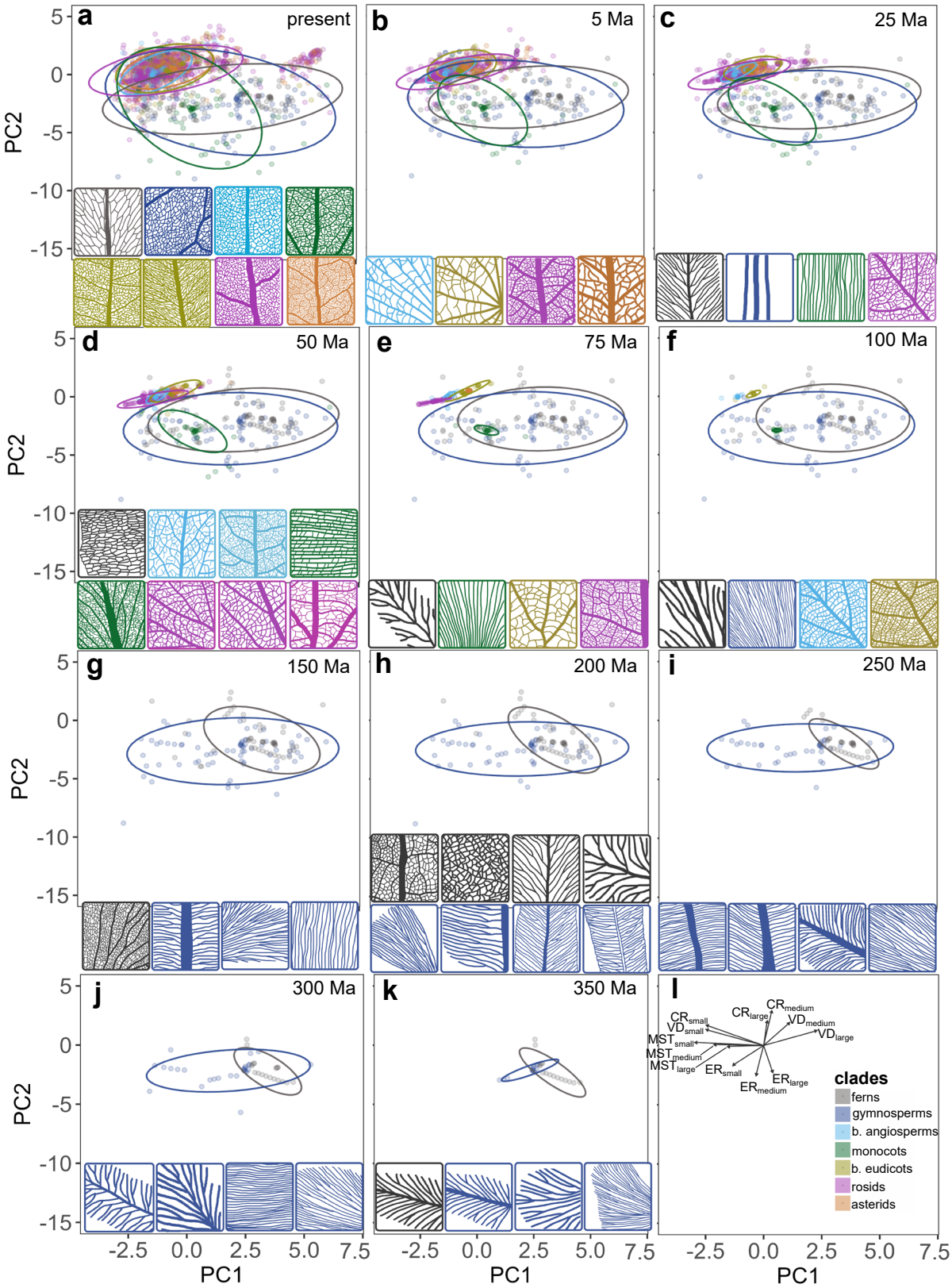

Extended Data Fig. 5 | Cumulative occupation of the venation architectural spaces for different plant clades over the geological time. First (PC1) and second (PC2) principal components of leaf venation architecture traits (*VD*, *MST*, *ER*, *CR*) at three vein sizes (small, medium, large) across plant clades. (**a**) Present; (**b**) 5 million years ago (Ma); (**c**) 25 Ma; (**d**) 50 Ma; (**e**) 75 Ma; (**f**) 100 Ma; (**g**) 150 Ma; (**h**) 200 Ma; (**i**) 250 Ma; (**j**) 300 Ma; (**k**) 350 Ma; (**l**) PCA loadings separated from the PCA scored for ease of visualization. 95% confidence ellipses enclose the data at each clade. Colored inserts illustrate some of the changes in architectural designs over time.

https://doi.org/10.1038/s41477-025-02011-y

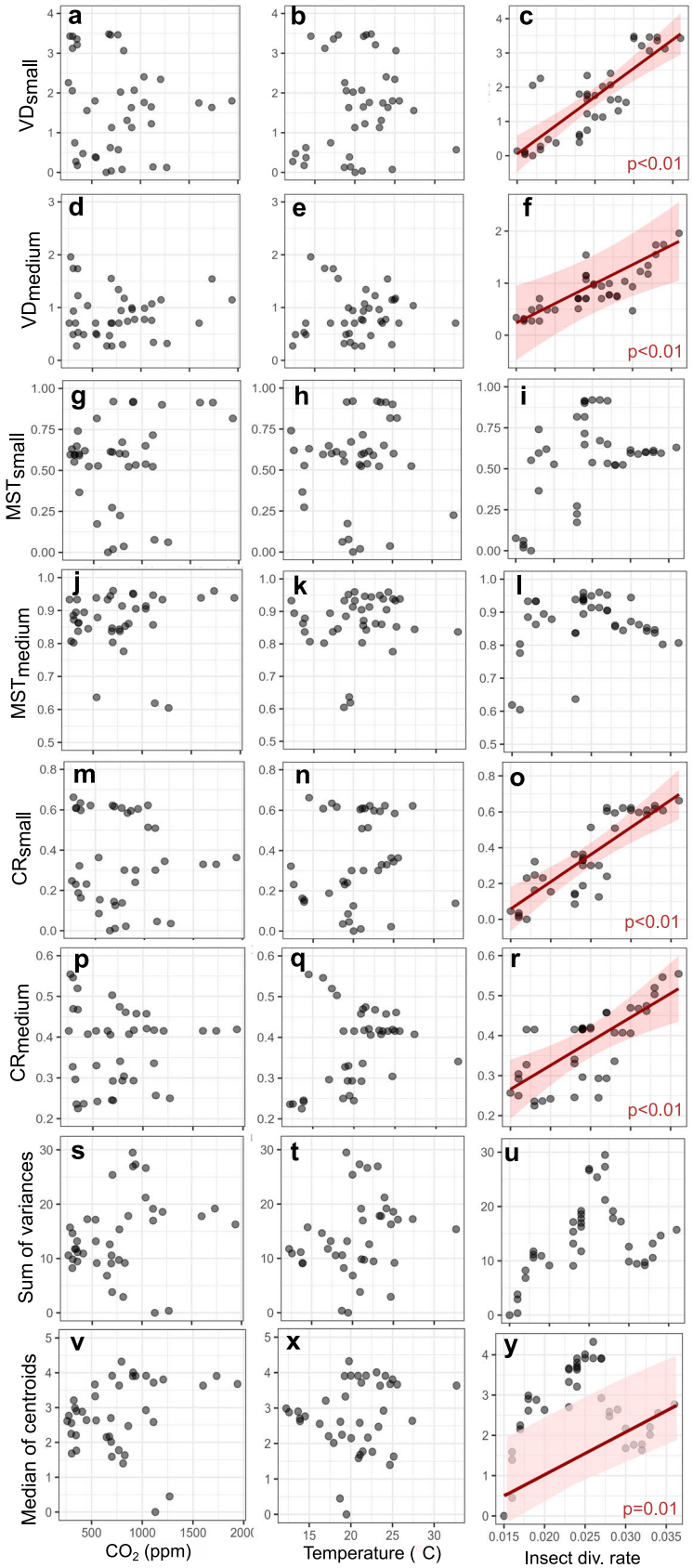

Extended Data Fig. 6 | Results of time-series analysis for identifying potential abiotic (global CO_2 atmospheric concentration and global mean temperature) and biotic (insect diversification rates) drivers of leaf venation architecture evolution in vascular plants. Vein density (*VD*, mm mm^{-2}) of small (**a-c**) and medium (**d-f**) veins; Minimum spanning tree ratio (*MST*) of small (**g-i**) and medium (**j-l**) veins; Loop circularity ratio (*CR*) of small (**m-o**) and medium (**p-r**) veins; Disparity metrics of sum of variances (**s-u**) and median of centroids (**v-y**). Venation traits (*VD, MST, CR*) depicted in **a-r** were obtained by collating ancestral state estimates at the phylogenetic tree internal nodes to measured trait values at the tree tips.

nature portfolio

Corresponding author(s): Ilaine Silveira Matos

Last updated by author(s): 2025/04/09

Reporting Summary

Nature Portfolio wishes to improve the reproducibility of the work that we publish. This form provides structure for consistency and transparency in reporting. For further information on Nature Portfolio policies, see our Editorial Policies and the Editorial Policy Checklist.

Statistics

For all statistical analyses, confirm that the following items are present in the figure legend, table legend, main text, or Methods section.

n/a	Confirmed	
☐	☒	The exact sample size (*n*) for each experimental group/condition, given as a discrete number and unit of measurement
☐	☒	A statement on whether measurements were taken from distinct samples or whether the same sample was measured repeatedly
☐	☒	The statistical test(s) used AND whether they are one- or two-sided *Only common tests should be described solely by name; describe more complex techniques in the Methods section.*
☐	☒	A description of all covariates tested
☐	☒	A description of any assumptions or corrections, such as tests of normality and adjustment for multiple comparisons
☐	☒	A full description of the statistical parameters including central tendency (e.g. means) or other basic estimates (e.g. regression coefficient) AND variation (e.g. standard deviation) or associated estimates of uncertainty (e.g. confidence intervals)
☐	☒	For null hypothesis testing, the test statistic (e.g. *F*, *t*, *r*) with confidence intervals, effect sizes, degrees of freedom and *P* value noted *Give P values as exact values whenever suitable.*
☐	☒	For Bayesian analysis, information on the choice of priors and Markov chain Monte Carlo settings
☐	☒	For hierarchical and complex designs, identification of the appropriate level for tests and full reporting of outcomes
☒	☐	Estimates of effect sizes (e.g. Cohen's *d*, Pearson's *r*), indicating how they were calculated

Our web collection on statistics for biologists contains articles on many of the points above.

Software and code

Policy information about availability of computer code

Data collection	GIMP version 2.10.32 (https://www.gimp.org/downloads/) and ImageJ version 1.53t (https://imagej.nih.gov/) were used to pre-process all leaf images. Leaf venation segmentation and calculation of venation architectural traits were conducted in LeafVeinCNN program versions 1.0.758 and 2.1243.
Data analysis	All analyses were carried out using R version 4.3.1. R-scripts to reproduce all analysis are publicly available on Zenodo (10.5281/zenodo.13300782).

For manuscripts utilizing custom algorithms or software that are central to the research but not yet described in published literature, software must be made available to editors and reviewers. We strongly encourage code deposition in a community repository (e.g. GitHub). See the Nature Portfolio guidelines for submitting code & software for further information.

Data

Policy information about availability of data

All manuscripts must include a data availability statement. This statement should provide the following information, where applicable:

- Accession codes, unique identifiers, or web links for publicly available datasets
- A description of any restrictions on data availability
- For clinical datasets or third party data, please ensure that the statement adheres to our policy

Data to reproduce all analysis will be made publicly available on Zenodo (10.5281/zenodo.13300782)65 upon acceptance of this manuscript. The original cleared

leaf images, leaf masks, extracted networks, and all LeafVeinCNN outputs for the 122 leaf samples collected at the University of California Botanical Garden at Berkeley are available at doi: 10.5061/dryad.1g1jwsv3666. Network segmentations and leaf masks of all other 878 samples are available at 10.5281/zenodo.13300782, as well as high-resolution cleared leaf images from Ecuador, Costa Rica, and University of California Museum of Paleontology collections. Original leaf cleared images of all other extant species are available at Wilf collection https://phytokeys.pensoft.net/article/72350/, Smithsonian National Cleared Leaf Collection https://collections.peabody.yale.edu/pb/nclc/. Original fossil leaf images are publicly available at https://peabody.yale.edu/; www.gbif.org; https://www.museumfuernaturkunde.berlin/; https://ucmpdb.berkeley.edu/, https://www.floridamuseum.ufl.edu/, https://search.museums.ualberta.ca/, https://ucmp.berkeley.edu/collections/paleobotany-collection/, https://phytokeys.pensoft.net/article/72350/,https://doi.org/10.1016/j.palwor.2017.01.003, https://doi.org/10.1080/14772019.2014.936974, https://doi.org/10.1080/11035890902857846, https://doi.org/10.1016/j.revpalbo.2009.08.004, https://doi.org/10.1016/j.revpalbo.2017.08.003, https://doi.org/10.1515/acpa-2017-0012, https://api.semanticscholar.org/CorpusID:135128574. World Plants (https://worldplants.de/), Paleobiology (https://paleobiodb.org/) and Fossilworks (fossilworks.org) databases were used to standardize species names. TimeTree: the timescale of life (https://timetree.org/) database was used to recalibrate the age of internal nodes of the phylogenetic tree.

Research involving human participants, their data, or biological material

Policy information about studies with human participants or human data. See also policy information about sex, gender (identity/presentation), and sexual orientation and race, ethnicity and racism.

Reporting on sex and gender	Does not apply
Reporting on race, ethnicity, or other socially relevant groupings	Does not apply
Population characteristics	Does not apply
Recruitment	Does not apply
Ethics oversight	Does not apply

Note that full information on the approval of the study protocol must also be provided in the manuscript.

Field-specific reporting

Please select the one below that is the best fit for your research. If you are not sure, read the appropriate sections before making your selection.

☐ Life sciences ☐ Behavioural & social sciences ☒ Ecological, evolutionary & environmental sciences

For a reference copy of the document with all sections, see nature.com/documents/nr-reporting-summary-flat.pdf

Ecological, evolutionary & environmental sciences study design

All studies must disclose on these points even when the disclosure is negative.

Study description	We used data from 1,000 extant and extinct plants to phylogenetically reconstruct ca. 400 Myr of venation evolutionary dynamics across plant clades and vein sizes. Leaf cleared images (extant species) and leaf fossil impressions (extinct species) were gathered from different collections. LeafVeinCNN program was used to segment the venation network and to calculate key venation architectural traits at multiple vein sizes. Standard R-packages were used to create a phylogenetic tree for all 1,000 taxa. Next, phylogenetic ridge regressions were used to investigate evolutionary trends in those architectural traits across the geological time, plant clades, and vein sizes. Disparity analysis were used to evaluate patterns of trait diversification over time. Generalized least squares regression analysis was used to identify protential abiotic and biotic drivers of leaf venation evolution.
Research sample	1,000 phylogenetically distinct extant and extinct plant taxa. The original cleared leaf images, leaf masks, extracted networks an all LeafVeinCNN outputs for the 122 leaf samples collected at the University of California Botanical Garden at Berkeley are available at doi: 10.5061/dryad.1g1jwsv3666. Network segmentations and leaf masks of all other 878 samples are available at 10.5281/zenodo.13300782, as well as high-resolution cleared leaf images from Ecuador, Costa Rica, and University of California Museum of Paleontology collections. Original leaf cleared images of all other extant species are available at Wilf collection https://phytokeys.pensoft.net/article/72350/, Smithsonian National Cleared Leaf Collection https://collections.peabody.yale.edu/pb/nclc/. Original fossil leaf images are publicly available at https://peabody.yale.edu/; www.gbif.org; https://www.museumfuernaturkunde.berlin/; https://ucmpdb.berkeley.edu/, https://www.floridamuseum.ufl.edu/, https://search.museums.ualberta.ca/, https://ucmp.berkeley.edu/collections/paleobotany-collection/, https://phytokeys.pensoft.net/article/72350/,https://doi.org/10.1016/j.palwor.2017.01.003, https://doi.org/10.1080/14772019.2014.936974, https://doi.org/10.1080/11035890902857846, https://doi.org/10.1016/j.revpalbo.2009.08.004, https://doi.org/10.1016/j.revpalbo.2017.08.003, https://doi.org/10.1515/acpa-2017-0012, https://api.semanticscholar.org/CorpusID:135128574. World Plants (https://worldplants.de/), Paleobiology (https://paleobiodb.org/) and Fossilworks (fossilworks.org) databases were used to standardize species names. TimeTree: the timescale of life (https://timetree.org/) database was used to recalibrate the age of internal nodes of the phylogenetic tree.
Sampling strategy	We gathered leaf cleared images of extant plant taxa and leaf fossil impressions of extinct taxa from diverse collections. We selected images with good enough resolution to observe minor veins. Our sampling strategy aimed to maximize the number of plant families/orders investigated and to balance the number of taxa per clade.

Data collection	Images of cleared leaves and fossil leaf impressions were gathered from duverse databases listed above.
Timing and spatial scale	Leaf images were gathered from diverse databases/collections from 2021-2023.
Data exclusions	Our initial database of pre-selected leaf images was over representing the rosids clade. So ~100 leaf images in this clade were excluded to result in a more balanced sampling size across clades. We excluded congeneric species whole leaf images had lower resolution and/or more damages (e.g. folds, bubbles, herbivory damage).
Reproducibility	Uncertainty in tips and nodes ages were accounted for in our analysis via bootstrapping methods using the "ovefitRR" function from the "RRphylo" R-package.
Randomization	Our analysis were conducted for the whole phylogenetic tree or for each major plant clade. The most updated phylogenetic classification was used to separate species into clades. Segmented veins were classified into 3 size classes (small, medium, and large). Because the range of vein widths largely vary across leaf samples and many samples exhibit vein tapering (i.e. veins become gradually smaller), there was no easy way to assign each segmented vein to a specific vein order. Thus, instead of using vein orders, we classified vein widths into 3 size classes based on their relative sizes.
Blinding	Not relevant.

Did the study involve field work? ☐ Yes ☒ No

Reporting for specific materials, systems and methods

We require information from authors about some types of materials, experimental systems and methods used in many studies. Here, indicate whether each material, system or method listed is relevant to your study. If you are not sure if a list item applies to your research, read the appropriate section before selecting a response.

Materials & experimental systems

n/a	Involved in the study
☒	☐ Antibodies
☒	☐ Eukaryotic cell lines
☐	☒ Palaeontology and archaeology
☒	☐ Animals and other organisms
☒	☐ Clinical data
☒	☐ Dual use research of concern
☐	☒ Plants

Methods

n/a	Involved in the study
☒	☐ ChIP-seq
☒	☐ Flow cytometry
☒	☐ MRI-based neuroimaging

Palaeontology and Archaeology

Specimen provenance	Leaf fossil impression images used in this study were obtained from publicly available collections or databases.
Specimen deposition	Original fossil leaf images are publicly available at https://peabody.yale.edu/; www.gbif.org; https://www.museumfuernaturkunde.berlin/; https://ucmpdb.berkeley.edu/, https://www.floridamuseum.ufl.edu/, https://search.museums.ualberta.ca/, https://ucmp.berkeley.edu/collections/paleobotany-collection/, https://phytokeys.pensoft.net/article/72350/,https://doi.org/10.1016/j.palwor.2017.01.003, https://doi.org/10.1080/14772019.2014.936974, https://doi.org/10.1080/11035890902857846, https://doi.org/10.1016/j.revpalbo.2009.08.004, https://doi.org/10.1016/j.revpalbo.2017.08.003, https://doi.org/10.1515/acpa-2017-0012, https://api.semanticscholar.org/CorpusID:135128574.
Dating methods	Fossil species approximate least appearance ages were obtained from Paleobiology and Fossilworks databases.

☒ Tick this box to confirm that the raw and calibrated dates are available in the paper or in Supplementary Information.

Ethics oversight	No ethical approval was required for this study, as it did not involve collection of any new plant/fossil material.

Note that full information on the approval of the study protocol must also be provided in the manuscript.

Dual use research of concern

Policy information about dual use research of concern

Hazards

Could the accidental, deliberate or reckless misuse of agents or technologies generated in the work, or the application of information presented in the manuscript, pose a threat to:

No	Yes	
☒	☐	Public health
☒	☐	National security
☒	☐	Crops and/or livestock
☒	☐	Ecosystems
☒	☐	Any other significant area

Experiments of concern

Does the work involve any of these experiments of concern:

No	Yes	
☒	☐	Demonstrate how to render a vaccine ineffective
☒	☐	Confer resistance to therapeutically useful antibiotics or antiviral agents
☒	☐	Enhance the virulence of a pathogen or render a nonpathogen virulent
☒	☐	Increase transmissibility of a pathogen
☒	☐	Alter the host range of a pathogen
☒	☐	Enable evasion of diagnostic/detection modalities
☒	☐	Enable the weaponization of a biological agent or toxin
☒	☐	Any other potentially harmful combination of experiments and agents

Plants

Seed stocks	This study did not use any live plant material. It only used cleared leaf or fossil compression images already archived in publicly available collections/databases.
Novel plant genotypes	Does not apply.
Authentication	Does not apply.